Hindawi Publishing Corporation
Mathematical Problems in Engineering
Volume 2009, Article ID 298906, 40 pages
doi:10.1155/2009/298906

Research Article

Motion Switching and Chaos of a Particle in a Generalized Fermi-Acceleration Oscillator

A. C. J. Luo and Y. Guo

Department of Mechanical and Industrial Engineering, Southern Illinois University Edwardsville, Edwardsville, IL 62026-1805, USA

Correspondence should be addressed to A. C. J. Luo, aluo@siue.edu

Received 23 September 2008; Revised 21 December 2008; Accepted 26 January 2009

Recommended by Edson Denis Leonel

Dynamic behaviors of a particle (or a bouncing ball) in a generalized Fermi-acceleration oscillator are investigated. The motion switching of a particle in the Fermi-oscillator causes the complexity and unpredictability of motion. Thus, the mechanism of motion switching of a particle in such a generalized Fermi-oscillator is studied through the theory of discontinuous dynamical systems, and the corresponding analytical conditions for the motion switching are developed. From solutions of linear systems in subdomains, four generic mappings are introduced, and mapping structures for periodic motions can be constructed. Thus, periodic motions in the Fermi-acceleration oscillator are predicted analytically, and the corresponding local stability and bifurcations are also discussed. From the analytical prediction, parameter maps of periodic and chaotic motions are achieved for a global view of motion behaviors in the Fermi-acceleration oscillator. Numerical simulations are carried out for illustrations of periodic and chaotic motions in such an oscillator. In existing results, motion switching in the Fermi-acceleration oscillator is not considered. The motion switching for many motion states of the Fermi-acceleration oscillator is presented for the first time. This methodology will provide a useful way to determine dynamical behaviors in the Fermi-acceleration oscillator.

1. Introduction

The Fermi-acceleration oscillator was first presented [1] by Fermi in 1949, which was used to explain the very high energy of cosmic ray. Since then, such an oscillator has been extensively investigated to interpret many physical and mechanical phenomena. In 1961, Ulam [2] pointed out the statistical properties of a particle in the Fermi-oscillator. In 1964, Zaslavskii and Chirikov [3] gave a comprehensive study of the Fermi-acceleration mechanism in the one-dimensional case. In 1972, Lieberman and Lichtenberg [4] discussed the stochastic and adiabatic behaviors of particles accelerated by periodic forcing, but such analysis was

based on the model presented by Zaslavskii and and Chirikov [3]. The corresponding stability of periodic motion was discussed. Such results can be found from Lichtenberg and Lieberman [5]. In 1978, Pustyl'nikov [6] discussed the reducibility of non-autonomous systems to normal forms in the neighborhood of an equilibrium point, and in 1995 he gave a detailed description about the Fermi-acceleration mechanism [7]. In 1986, Jose and Cordery [8] studied a quantum Fermi-accelerator consisting of a particle moving between a fixed wall and a periodic oscillator. In 1987, Celaschi and Zimmerman [9] gave an experimental investigation to observe the period-doubling route to chaos for a 1D system with two parameters. In 1988, Kowalik et al. [10] completed an experimental investigation on chaotic behaviors of a ball in the bouncing ball system, and used the Zaslavski's mapping to analyze such chaotic behaviors. In 1989, Luna-Acosta [11] investigated the dynamics of the Fermi-accelerator subject to a viscous friction. In 1996, Warr et al. [12] determined experimentally a probability distribution function for a single-particle vibrating in one dimension. In 1998, Saif et al. [13] studied the dynamics of both classical and quantum Fermi-acceleration oscillators and determined the dynamical localization of position and momentum for a modulation amplitude. Lopac and Dananić [14] investigated chaotic dynamics and energy conservation in a gravitationally driven Fermi-accelerator. In 2004, Bouchet et al. [15] presented a simple stochastic system to generate anomalous diffusion of both position and velocity for the Fermi-accelerator. Leonel et al. [16] completed a scaling analysis of chaotic motion in the Fermi-Ulam-simplified accelerator, and Leonel et al. [17] investigated the effect of a time-dependent perturbation on a Fermi-accelerator model using discrete dynamical systems. In 2006, Leonel and McClintock [18] discussed the influence of dissipation on a simplified Fermi-Ulam accelerator model. In 2007, Leonel and de Carvalho [19] presented the Fermi-accelerator model with inelastic collisions through a two-dimensional nonlinear area-contracting map. In 2007, Karlis et al. [20] investigated the Fermi-acceleration of an ensemble of noninteracted particles in two stochastic two-moving walls in the Fermi-Ulam model. Leonel and Silva [21] discussed the dynamical properties of a prototype for the Fermi-acceleration modeled by two nonlinear terms. Kamphorst et al. [22] numerically studied the energy change of a particle bouncing in a time-varying billiard. In 2008, Leonel and Livorati [23] presented the average velocity behavior on a dissipative Fermi-acceleration model with a scaling approach. The scaling characteristics of a breathing circular billiard were investigated by Ladeira and da Silva [24]. All the aforesaid investigations were based on the one motion state with impact. The motion switching was not considered. In this paper, the motion switching from a motion state into another one will be investigated.

The similar studies of impacting systems have also been carried out in mechanical engineering because the impact is an important phenomenon in mechanical engineering. For instance, in 1982, Holmes [25] investigated the dynamics of repeated impacts of a ball with a sinusoidal vibrating table. It was assumed that the mass of the ball is much smaller than the mass of the table, and the ball and table always impact at the same position. In 1983, Bapat et al. [26] investigated the asymptotically stable periodic motions of a ball in an impact-pair. Shaw and Holmes [27] studied harmonic, subharmonic, and chaotic motions of a single-degree-of-freedom nonlinear oscillator and analyzed the corresponding bifurcations. In 1987, Whiston [28] studied the steady-state, vibroimpacting responses of one-dimensional, harmonically excited, linear oscillator. In 1988, C. N. Bapat and C. Bapat [29] used Fourier series and perturbation method to determine the stability regions of two equispaced impact motion of an impact-pair under a prescribed periodic displacement. In 1991, Nordmark [30] studied the singularity caused by grazing impact in a single degree of freedom impact oscillator. In 1992, Foale and Bishop [31] investigated a periodically forced linear oscillator

with instantaneous impacts at one or two stops. In 1994, Budd and Dux [32] investigated the chattering behavior of a periodically forced, single-degree-of-freedom impact oscillator with a restitution law for each impact. Foale [33] tried to determine bifurcations in a periodically driven impact oscillator analytically, and the impact wall is fixed. In 1995, Bapat [34] studied the motion of an inclined impact damper with friction and collision on both sides. In order to understand dynamical behaviors of a bouncing ball on a vibrating table, in 1996, Luo and Han [35] presented a reasonable model and analytically predicted the periodic motions. In 2002, Luo [36] investigated the stability and bifurcation of unsymmetrical periodic motions in a horizontal impact oscillator with a periodic excitation. In 2004, Giusepponi et al. [37] discussed the randomness of motion of the bouncing ball on a sinusoidally vibrating table. Luo [38] discussed the stability, saddle-node and period-doubling bifurcations for the LR model motion in a horizontal impact oscillator.

In 2005, Luo [39] presented the mapping dynamics of periodic motions in a nonsmooth piecewise system. To understand the complexity in discontinuous dynamical systems, Luo [40, 41] developed a theory of the non-smooth dynamical systems on connectable and accessible subdomains. Luo and Chen [42] applied such a theory to investigate the grazing bifurcation and periodic motions in an idealized gear-transmission system with impacts. In 2006, Luo and Gegg [43] used such a theory to develop the force criteria of stick and nonstick motion in harmonically forced, friction-induced oscillators. In 2007, Luo [44] discussed switching bifurcations of a flow to the separation boundary. Luo and Rapp [45] studied the switching dynamics of a flow from one domain into another adjacent domain in a periodically driven, discontinuous dynamical system. Luo and O'Connor [46, 47] discussed the dynamics mechanism of impact chatters and possible stick motions in a gear transmission system, and the moving boundaries are controlled by other dynamical systems. In the gear model, the two boundaries are movable. However, the Fermi-acceleration oscillator possesses both static and time-varying boundaries in phase space for impacts and motion switching. In existing investigations on the Fermi-acceleration oscillator or impact oscillators, the dynamical systems are not switched except for impacts. Thus, in this paper, the impacting and sticking of two systems on the boundaries will be considered, which will provide a practical model to predict the motions of the Fermi-acceleration oscillator.

This paper will investigate dynamics of a generalized Fermi-acceleration oscillator. The domains and boundaries for such a problem will be introduced because of the discontinuity, and the analytical conditions of stick and grazing motions will be developed at the boundaries. The mapping technique will be used for the analytical prediction of periodic motions of the extended Fermi-acceleration oscillator. The local stability and bifurcation of periodic motions will be discussed using the eigenvalue analysis. Bifurcation scenario and analytical prediction of motions will be presented, and numerical simulations of periodic and chaotic motions will be carried out. In addition, the Poincare mapping sections will be presented for illustrations of chaotic motions, and the parameter maps will be presented as well.

2. Physical Problem Statement

A generalized Fermi-acceleration oscillator consists of a particle moving vertically between a fixed wall and the moving piston in a vibrating oscillator. The piston of mass m_2 is connected with a spring of constant k and a damper with coefficient c, and they are set on a periodically oscillating base, as shown in Figure 1. The mass of particle is m_1 and the

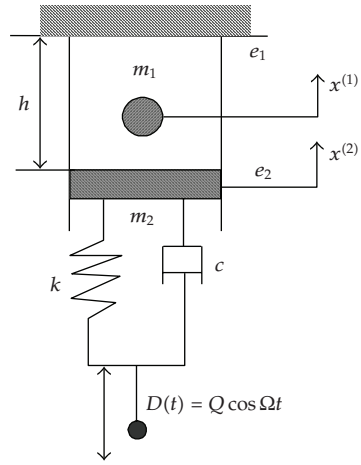

Figure 1: Mechanical model.

restitution coefficients of impact are e_1 and e_2 for the wall and piston, respectively. The gap between the fixed wall and the equilibrium position of piston is h. The displacement of the oscillating base is $D(t) = Q\cos\Omega t$.

If the particle does not stay on the piston, the corresponding motion of such a system is called the *nonstick motion*. For this case, the equation of motion for such a system is given from the Newton's law, that is,

$$\begin{aligned} \ddot{x}^{(1)} &= -g, \\ \ddot{x}^{(2)} + 2d^{(2)}\dot{x}^{(2)} + \left(\omega^{(2)}\right)^2 x^{(2)} &= \left(\omega^{(2)}\right)^2 Q\cos\Omega t - 2d^{(2)}Q\Omega\sin\Omega t, \end{aligned} \tag{2.1}$$

where $d^{(2)} = c/2m_2$, and $\omega^{(2)} = \sqrt{k/m_2}$. $\ddot{x}^{(i)}$, $\dot{x}^{(i)}$ and $x^{(i)}$ $(i = 1, 2)$ are acceleration, velocity, and displacement, respectively. g is the gravitational acceleration. The superscripts $i = 1$ and 2 represent the particle and piston, accordingly.

If the particle stays on the piston and they move together, such a motion is called *the stick motion*. For the stick motion, there is a relation ($x^{(1)} = x^{(2)}$ and $\dot{x}^{(1)} = \dot{x}^{(2)}$) and the corresponding equation of motion becomes

$$\ddot{x}^{(i)} + 2d^{(0)}\dot{x}^{(i)} + \left(\omega^{(0)}\right)^2 x^{(i)} = \left(\omega^{(0)}\right)^2 Q\cos\Omega t - 2d^{(0)}Q\Omega\sin\Omega t, \tag{2.2}$$

where $d^{(0)} = c/2(m_1 + m_2)$, $\omega^{(0)} = \sqrt{k/(m_1 + m_2)}$. The superscripts $i = 1, 2$ represent the particle and piston, respectively.

For nonstick motion, the impact relation between the particle and the fixed wall is

$$\begin{aligned} x_+^{(1)} = x_-^{(1)} = h, \qquad \dot{x}_+^{(1)} = -e_1\dot{x}_-^{(1)}, \\ x_+^{(2)} = x_-^{(2)}, \qquad \dot{x}_+^{(2)} = \dot{x}_-^{(2)}, \end{aligned} \tag{2.3}$$

where (+) and (−) represent the after and before impact. The impact relations between the particle and the vibrating piston are

$$\begin{aligned} x_+^{(1)} &= x_+^{(2)} = x_-^{(1)} = x_-^{(2)}, \\ \dot{x}_+^{(1)} &= \frac{m_1\dot{x}_-^{(1)} + m_2\dot{x}_-^{(2)} - m_2e_2\left(\dot{x}_-^{(1)} - \dot{x}_-^{(2)}\right)}{m_1 + m_2}, \\ \dot{x}_+^{(2)} &= \frac{m_1\dot{x}_-^{(1)} + m_2\dot{x}_-^{(2)} + m_1e_2\left(\dot{x}_-^{(1)} - \dot{x}_-^{(2)}\right)}{m_1 + m_2}. \end{aligned} \tag{2.4}$$

3. Analytical Conditions

In this section, the domains and boundaries of the extended Fermi-oscillator will be introduced in the absolute and relative coordinates. From such domains and boundaries, the analytical conditions of stick and grazing motions to each switching boundary will be developed from the theory of discontinuous dynamical systems.

3.1. Domains and Boundaries for Absolute Motions

To analyze the motion discontinuity in the Fermi-acceleration oscillator, the origin of the absolute coordinates is set at the equilibrium of piston. The domains for the particle and piston without stick in the absolute coordinates are defined as

$$\begin{aligned} \Omega_1^{(1)} &= \left\{\left(x^{(1)}, \dot{x}^{(1)}\right) \mid x^{(1)} \in \left(x^{(2)}, h\right)\right\}, \\ \Omega_1^{(2)} &= \left\{\left(x^{(2)}, \dot{x}^{(2)}\right) \mid x^{(2)} \in \left(-\infty, x^{(1)}\right)\right\}. \end{aligned} \tag{3.1}$$

The corresponding boundaries are defined as

$$\begin{aligned} \partial\Omega_{1(+\infty)}^{(i)} &= \left\{\left(x^{(i)}, \dot{x}^{(i)}\right) \middle| \varphi_{1(+\infty)}^{(1)} \equiv x^{(1)} - h = 0,\ \dot{x}^{(1)} \neq 0\right\}, \\ \partial\Omega_{1(-\infty)}^{(i)} &= \left\{\left(x^{(i)}, \dot{x}^{(i)}\right) \middle| \varphi_{1(-\infty)}^{(i)} \equiv x^{(i)} - x^{(\bar{i})} = 0,\ \dot{x}^{(i)} \neq \dot{x}^{(\bar{i})}\right\}, \end{aligned} \tag{3.2}$$

where $\bar{i} = 1$ and 2 are for $i = 2$ and 1, accordingly. The subscripts "$\pm\infty$" represent the permanent boundaries at $x^{(1)} = h$ and $x^{(i)} = x^{(\bar{i})}$. If a flow in a subdomain of a dynamical system cannot pass over a switching boundary into another subdomain without any transport law, such a boundary is called the permanent boundary (e.g., Luo [48]). For this problem, the impact law, as a transport law, should be applied for such permanent boundaries. In other words, the impact relations in (2.3) and (2.4) will be applied for such permanent boundaries. The subdomains and boundaries for motions of particle and piston in phase space are sketched in Figure 2. The subdomains are filled with diagonal lines. The boundary ($\partial\Omega_{1(+\infty)}^{(1)}$) for the particle is a dashed line with $x^{(1)} = h$ and the boundaries ($\partial\Omega_{1(-\infty)}^{(1)}$ and $\partial\Omega_{1(-\infty)}^{(2)}$) with $x^{(1)} = x^{(2)}$ for the particle and piston are two dashed curves.

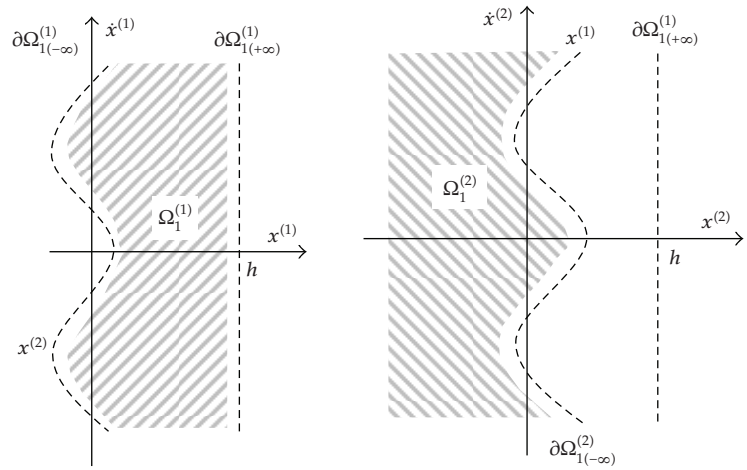

Figure 2: Absolute domains and boundaries without stick: (a) particle and (b) piston.

For this system, there is a stick motion of the particle and piston. Thus, the stick motion will appear and vanish under certain conditions. Such onset and disappearance of the sticking motion will generate new boundaries and domains. The domains $\Omega_0^{(i)}$ and $\Omega_1^{(i)}$ $(i = 1, 2)$ for the particle and piston with stick in the absolute coordinates are defined as

$$\begin{aligned}
\Omega_0^{(1)} &= \left\{ \left(x^{(1)}, \dot{x}^{(1)}\right) \mid x^{(1)} \in \left(-\infty, x_{cr}^{(2)}\right), \dot{x}^{(1)} = \dot{x}^{(2)} \right\}, \\
\Omega_0^{(2)} &= \left\{ \left(x^{(2)}, \dot{x}^{(2)}\right) \mid x^{(2)} \in \left(x^{(1)}, h\right), \dot{x}^{(1)} = \dot{x}^{(2)} \right\}, \\
\Omega_1^{(1)} &= \left\{ \left(x^{(1)}, \dot{x}^{(1)}\right) \mid x^{(1)} \in \left(x_{cr}^{(2)}, h\right), \dot{x}^{(1)} \neq \dot{x}^{(2)} \right\}, \\
\Omega_1^{(2)} &= \left\{ \left(x^{(2)}, \dot{x}^{(2)}\right) \mid x^{(2)} \in \left(-\infty, x_{cr}^{(1)}\right), \dot{x}^{(1)} \neq \dot{x}^{(2)} \right\}.
\end{aligned} \tag{3.3}$$

The corresponding boundaries are defined as

$$\begin{aligned}
\partial\Omega_{1(+\infty)}^{(i)} &= \left\{ \left(x^{(i)}, \dot{x}^{(i)}\right) \middle| \varphi_{1(+\infty)}^{(1)} \equiv x^{(1)} - h = 0, \dot{x}^{(1)} \neq 0 \right\}, \\
\partial\Omega_{10}^{(i)} &= \left\{ \left(x^{(i)}, \dot{x}^{(i)}\right) \middle| \varphi_{10}^{(i)} \equiv x^{(i)} - x_{cr}^{(\bar{i})} = 0, \dot{x}^{(i)} = \dot{x}_{cr}^{(\bar{i})} \right\},
\end{aligned} \tag{3.4}$$

where $x_{cr}^{(i)}$ is an instantaneous value for the appearance or vanishing of stick motion with $\dot{x}_{cr}^{(1)} = \dot{x}_{cr}^{(2)}$ and $x_{cr}^{(1)} = x_{cr}^{(2)}$. The instantaneous values are dependent on time, which cannot give specified values. The domains ($\Omega_1^{(i)}$ and $\Omega_0^{(i)}$) describe the domains for the nonstick and stick motions of the particle and piston, respectively. $\partial\Omega_{1(-\infty)}^{(1)}$ is the impact chatter boundary for the particle impacting with the piston, and $\partial\Omega_{10}^{(1)}$ and $\partial\Omega_{01}^{(1)}$ are the stick onset and vanishing boundaries for the particle sticking with the piston. Similarly, $\partial\Omega_{1(-\infty)}^{(2)}$ is the impact chatter boundary for the piston impacting with the particle, and $\partial\Omega_{10}^{(2)}$ and $\partial\Omega_{01}^{(2)}$ are the stick onset and vanishing boundaries for the piston sticking with particle. In Figure 3, the nonstick

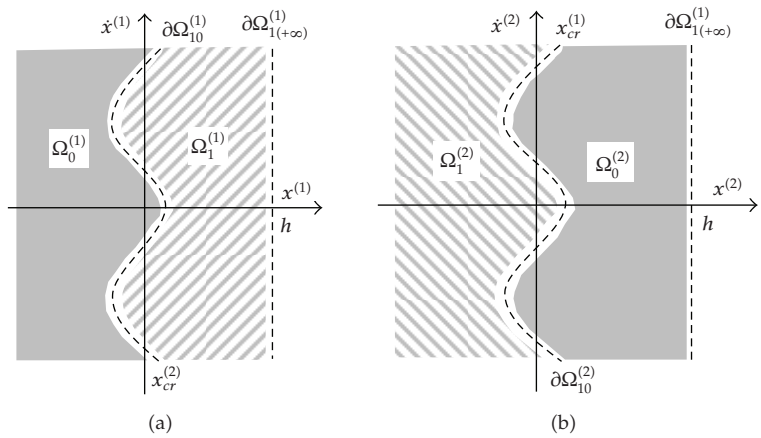

Figure 3: Absolute domains and boundaries with stick: (a) particle and (b) piston.

and stick domains ($\Omega_1^{(i)}$ and $\Omega_0^{(i)}$) are presented through the filled and shaded regions. The boundaries ($\partial\Omega_{10}^{(i)}$ and $\partial\Omega_{01}^{(i)}$, $i = 1,2$) for the particle and piston are given by the dashed curves in the absolute frame. The nonstick, permanent boundary ($\partial\Omega_{1(+\infty)}^{(1)}$) for the particle is a dashed line, and such a boundary is also applied for the piston as a permanent boundary.

From the aforedefined domains, the vectors for absolute motions are defined as

$$\mathbf{x}_\lambda^{(i)} = \left(x_\lambda^{(i)}, \dot{x}_\lambda^{(i)}\right)^T, \quad \mathbf{f}_\lambda^{(i)} = \left(\dot{x}_\lambda^{(i)}, F_\lambda^{(i)}\right)^T \quad \text{for } i = 1,2,\ \lambda = 0,1, \tag{3.5}$$

where the subscript ($\lambda = 0,1$) represents the corresponding domain. The equation of absolute motion of the generalized Fermi-oscillator is rewritten in a state vector form of

$$\dot{\mathbf{x}}_\lambda^{(i)} = \mathbf{f}_\lambda^{(i)}\left(\mathbf{x}_\lambda^{(i)}, t\right) \quad \text{for } i = 1,2,\ \lambda = 0,1, \tag{3.6}$$

and one obtains

$$\begin{aligned} F_1^{(1)}\left(x_1^{(1)}, t\right) &= -g, \\ F_1^{(2)}\left(x_1^{(2)}, t\right) &= -2d\dot{x}_1^{(2)} - \omega^2 x_1^{(2)} + \omega^2 Q\cos\Omega t - 2dQ\Omega\sin\Omega t \end{aligned} \tag{3.7}$$

for the nonstick motion, and

$$F_1^{(i)}\left(x_0^{(i)}, t\right) = -2d^{(0)}\dot{x}_0^{(i)} - \left(\omega^{(0)}\right)^2 x_0^{(i)} + \left(\omega^{(0)}\right)^2 Q\cos\Omega t - 2d^{(0)}Q\Omega\sin\Omega t \tag{3.8}$$

for the stick motion.

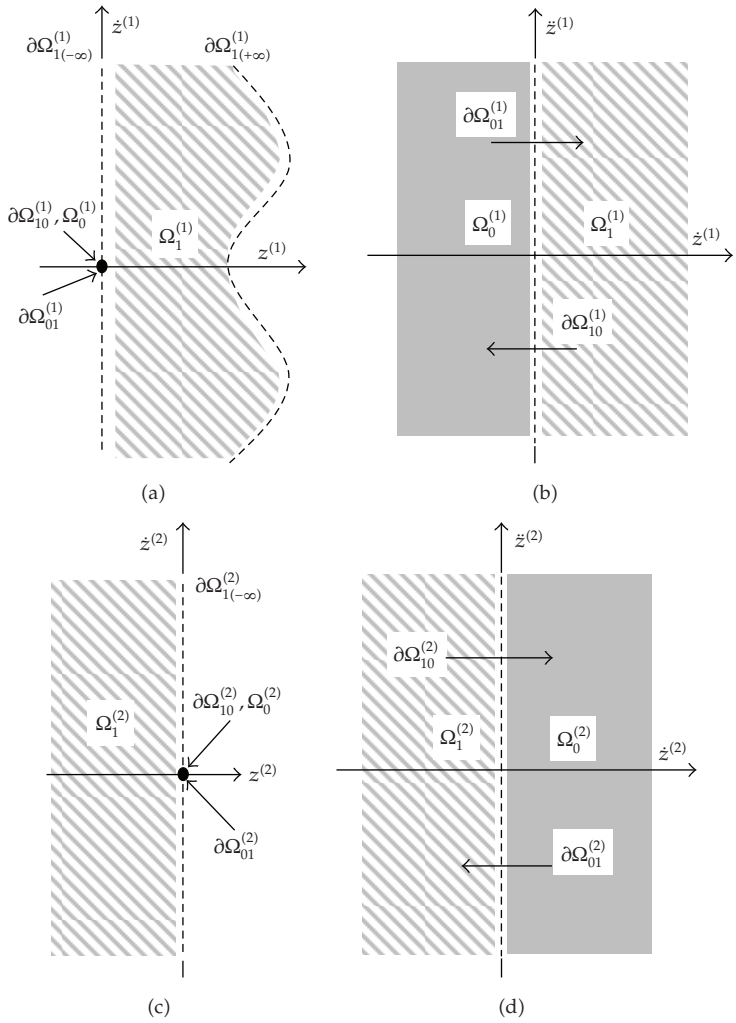

Figure 4: Relative domains and boundaries definition: (a) $(z, \dot{z})$-plane for particle, (b) $(\dot{z}, \ddot{z})$-plane for particle, (c) $(z, \dot{z})$-plane for piston, (d) $(\dot{z}, \ddot{z})$-plane for piston.

3.2. Domains and Boundaries for Relative Motions

Because the switching boundary varies with time, it is very difficult to develop the switching conditions. Thus, the relative coordinates for such a Fermi-oscillator are adopted herein. The relative displacement, relative velocity, and relative acceleration between the particle and the piston are $z^{(i)} = x^{(i)} - x^{(\bar{i})}$, $\dot{z}^{(i)} = \dot{x}^{(i)} - \dot{x}^{(\bar{i})}$, and $\ddot{z}^{(i)} = \ddot{x}^{(i)} - \ddot{x}^{(\bar{i})}$, where the index $i = 1, 2$ (with $\bar{i} = 2, 1$) represents the particle and piston, respectively. The stick domain and boundaries in the relative phase space become points, as shown in Figures 4(a) and 4(c). Because the piston and particle have the same displacement and velocity for the entire stick motion, the boundary and domains in the relative phase plane become zero. However, the relative interaction force between the particle and position are different before or after the stick. Thus, the plane of relative velocity and acceleration should be considered, and the stick domains and boundaries in the relative velocity and acceleration (i.e., $(\dot{z}^{(i)}, \ddot{z}^{(i)})$) are presented in

Figures 4(b) and 4(d). The filled domains are for stick motion. The shaded regions are for nonstick motion. The domains $\Omega_0^{(i)}$ and $\Omega_1^{(i)}$ for the relative motions of the particle and piston are defined as

$$\begin{aligned}
\Omega_0^{(i)} &= \left\{ \left(z^{(i)}, \dot{z}^{(i)} \right) \mid \dot{z}^{(i)} = 0, z^{(i)} = 0 \right\} \quad \text{for } i = 1, 2, \\
\Omega_1^{(1)} &= \left\{ \left(z^{(1)}, \dot{z}^{(1)} \right) \mid z^{(1)} \in \left(0, h - x^{(2)} \right) \right\}, \\
\Omega_1^{(2)} &= \left\{ \left(z^{(2)}, \dot{z}^{(2)} \right) \mid z^{(2)} \in (-\infty, 0) \right\}.
\end{aligned} \tag{3.9}$$

The boundaries $\partial\Omega_{1(+\infty)}^{(i)}$, $\partial\Omega_{1(-\infty)}^{(i)}$, $\partial\Omega_{10}^{(i)}$, and $\partial\Omega_{01}^{(i)}$ for the relative motions of the particle and piston are defined as

$$\begin{aligned}
\partial\Omega_{1(+\infty)}^{(i)} &= \left\{ \left(z^{(i)}, \dot{z}^{(i)} \right) \middle| \varphi_{1(+\infty)}^{(1)} \equiv z^{(1)} - h + x^{(2)} = 0 \right\}, \\
\partial\Omega_{1(-\infty)}^{(i)} &= \left\{ \left(z^{(i)}, \dot{z}^{(i)} \right) \middle| \varphi_{1(-\infty)}^{(i)} \equiv z^{(i)} = 0 \right\}, \\
\partial\Omega_{10}^{(i)} = \partial\Omega_{01}^{(i)} &= \left\{ \left(z^{(i)}, \dot{z}^{(i)} \right) \middle| \varphi_{10}^{(i)} \equiv \dot{z}_{cr}^{(i)} = 0, z_{cr}^{(i)} = 0 \right\},
\end{aligned} \tag{3.10}$$

where $\partial\Omega_{1(-\infty)}^{(1)}$ is the impact chatter boundary for the particle, and two stick boundaries for the particle are $\partial\Omega_{10}^{(1)}$ and $\partial\Omega_{01}^{(1)}$. Similarly, $\partial\Omega_{1(-\infty)}^{(2)}$ is the impact chatter boundary for the piston, and $\partial\Omega_{10}^{(2)}$ and $\partial\Omega_{01}^{(2)}$ are two stick boundaries for the piston. $\partial\Omega_{1(+\infty)}^{(i)}$ is the impact boundary for the particle and the fixed wall.

The vectors for relative motions are

$$\mathbf{z}_\lambda^{(i)} = \left(z_\lambda^{(i)}, \dot{z}_\lambda^{(i)} \right)^T, \qquad \mathbf{g}_\lambda^{(i)} = \dot{\mathbf{z}}_\lambda^{(i)} = \left(\dot{z}_\lambda^{(i)}, g_\lambda^{(i)} \right)^T, \tag{3.11}$$

where the superscript ($i = 1, 2$) represents the particle and piston, respectively. The subscript ($\lambda = 0, 1$) represents the corresponding domains. The equation of relative motion is rewritten in a vector form of

$$\dot{\mathbf{z}}_\lambda^{(i)} = \mathbf{g}_\lambda^{(i)} \left(\mathbf{z}_\lambda^{(i)}, \mathbf{x}_\lambda^{(\bar{i})}, t \right), \qquad \dot{\mathbf{x}}_\lambda^{(\bar{i})} = \mathbf{f}_\lambda^{(\bar{i})} \left(\mathbf{x}_\lambda^{(\bar{i})}, t \right), \tag{3.12}$$

where

$$\begin{aligned}
g_1^{(1)} \left(\mathbf{z}_1^{(1)}, \mathbf{x}_1^{(2)}, t \right) &= -g + 2d^{(2)} \dot{x}_1^{(2)} + \left(\omega^{(2)} \right)^2 x_1^{(2)} - \left(\omega^{(2)} \right)^2 Q \cos \Omega t + 2d^{(2)} Q \Omega \sin \Omega t, \\
g_1^{(2)} \left(\mathbf{z}_1^{(2)}, \mathbf{x}_1^{(1)}, t \right) &= -2d^{(2)} \dot{z}_1^{(2)} - \left(\omega^{(2)} \right)^2 z_1^{(2)} + \left(\omega^{(2)} \right)^2 Q \cos \Omega t - 2d^{(2)} Q \Omega \sin \Omega t \\
&\quad - 2d^{(2)} \dot{x}_1^{(1)} - \left(\omega^{(2)} \right)^2 x_1^{(1)} + g,
\end{aligned} \tag{3.13}$$

for nonstick motion

$$\begin{aligned} \dot{z}_0^{(i)} &= 0, \\ g_0^{(i)}\left(\mathbf{z}_0^{(i)}, \mathbf{x}_0^{(\bar{i})}, t\right) &= 0, \end{aligned} \qquad \text{for } i = 1,2 \text{ with } \bar{i} = 2,1, \tag{3.14}$$

for stick motion.

3.3. Analytical Conditions

The analytical conditions of stick and grazing motion will be developed from the theory of non-smooth dynamical systems in Luo [40, 41, 44, 49, 50]. The grazing motion is a motion tangential to the switching boundary in phase space. In the Fermi-acceleration oscillator, once the ball meets with the piston or the wall, there is a motion tangential to the switching boundary in phase space. Such a motion is called the grazing motion. To develop the analytical conditions of the grazing and stick motion to the switching boundaries, the normal vectors of such boundaries should be determined, that is,

$$\begin{aligned} \mathbf{n}_{\partial\Omega_{\alpha\beta}^{(i)}} &= \nabla\varphi_{\alpha\beta}^{(i)} = \left(\frac{\partial\varphi_{\alpha\beta}^{(i)}}{\partial z^{(i)}}, \frac{\partial\varphi_{\alpha\beta}^{(i)}}{\partial \dot{z}^{(i)}}\right)^T \quad \text{for the relative frame,} \\ \mathbf{n}_{\partial\Omega_{\alpha\beta}} &= \nabla\varphi_{\alpha\beta}^{(i)} = \left(\frac{\partial\varphi_{\alpha\beta}^{(i)}}{\partial x^{(i)}}, \frac{\partial\varphi_{\alpha\beta}^{(i)}}{\partial \dot{x}^{(i)}}\right)^T \quad \text{for the absolute frame.} \end{aligned} \tag{3.15}$$

The normal vectors to the stick boundaries $(\mathbf{n}_{\partial\Omega_{10}^{(1)}}, \mathbf{n}_{\partial\Omega_{01}^{(1)}})$ and impact boundary $(\mathbf{n}_{\partial\Omega_{1(+\infty)}^{(1)}}, \mathbf{n}_{\partial\Omega_{1(-\infty)}^{(1)}})$ are

$$\begin{aligned} \mathbf{n}_{\partial\Omega_{10}^{(1)}} = \mathbf{n}_{\partial\Omega_{01}^{(1)}} = (0,1)^T, \quad \mathbf{n}_{\partial\Omega_{1(-\infty)}^{(1)}} = (1,0)^T \quad \text{in the relative frame,} \\ \mathbf{n}_{\partial\Omega_{1(+\infty)}^{(1)}} = (1,0)^T \quad \text{in the absolute frame.} \end{aligned} \tag{3.16}$$

Before the analytical conditions are developed, the zero-order and first-order G-functions in the relative frame will be presented. For the straight-line boundary, the zero-order and first-order G-functions are given from Luo [49, 50], that is,

$$\begin{aligned} G_{\partial\Omega_{01}^{(i)}}^{(0,0)}\left(\mathbf{z}_0^{(i)}, t_{m\pm}\right) &= \mathbf{n}_{\partial\Omega_{01}^{(1)}}^T \cdot \mathbf{g}^{(i)}\left(\mathbf{z}_0^{(i)}, \mathbf{x}_0^{(\bar{i})}, t_{m\pm}\right) = g_0^{(i)}\left(\mathbf{z}_0^{(i)}, \mathbf{x}_0^{(\bar{i})}, t_{m\pm}\right) = \ddot{z}_0^{(i)}\left(t_{m\pm}\right), \\ G_{\partial\Omega_{10}^{(i)}}^{(0,1)}\left(\mathbf{z}_1^{(i)}, t_{m\pm}\right) &= \mathbf{n}_{\partial\Omega_{10}^{(1)}}^T \cdot \mathbf{g}^{(i)}\left(\mathbf{z}_1^{(i)}, \mathbf{x}_1^{(\bar{i})}, t_{m\pm}\right) = g_1^{(i)}\left(\mathbf{z}_1^{(i)}, \mathbf{x}_1^{(\bar{i})}, t_{m\pm}\right) = \ddot{z}_1^{(i)}\left(t_{m\pm}\right), \\ G_{\partial\Omega_{01}^{(i)}}^{(1,0)}\left(\mathbf{z}_0^{(i)}, t_{m\pm}\right) &= \mathbf{n}_{\partial\Omega_{01}^{(1)}}^T \cdot D\mathbf{g}^{(i)}\left(\mathbf{z}_0^{(i)}, \mathbf{x}_0^{(\bar{i})}, t_{m\pm}\right) = \frac{d}{dt} g_0^{(i)}\left(\mathbf{z}_0^{(i)}, \mathbf{x}_0^{(\bar{i})}, t\right)\Big|_{t=t_{m\pm}} = \dddot{z}_0^{(i)}\left(t_{m\pm}\right), \\ G_{\partial\Omega_{10}^{(i)}}^{(1,1)}\left(\mathbf{z}_1^{(i)}, t_{m\pm}\right) &= \mathbf{n}_{\partial\Omega_{10}^{(1)}}^T \cdot D\mathbf{g}^{(i)}\left(\mathbf{z}_1^{(i)}, \mathbf{x}_1^{(\bar{i})}, t_{m\pm}\right) = \frac{d}{dt} g_1^{(i)}\left(\mathbf{z}_1^{(i)}, \mathbf{x}_1^{(\bar{i})}, t\right)\Big|_{t=t_{m\pm}} = \dddot{z}_1^{(i)}\left(t_{m\pm}\right). \end{aligned} \tag{3.17}$$

Notice that the switching time t_m is the motion at the corresponding switching boundary, and $t_{m\pm} = t_m \pm 0$ represents the motion in domains rather than on the boundary. In $G^{(k,\lambda)}_{\partial\mathfrak{B}^{(i)}_1}$, two superscripts λ ($\lambda = 0, 1$) and k ($k = 0, 1$) represent the λ-subdomain and the kth order of G-functions, respectively. Again $i = 1$ and 2 are for the particle and piston. The zero-order G-function ($k = 0$) is the normal component of the vector field in the normal direction of boundary, and the first-order G-function ($k = 1$) is the time-change rate of the normal component of vector fields. The detailed discussion of G-functions can be referred to Luo [48–50]. Similarly, the G-functions for the impact boundaries are given by

$$\begin{aligned}
&G^{(0,1)}_{\partial\Omega^{(1)}_{1(+\infty)}}\left(\mathbf{x}^{(1)}_1, t_{m\pm}\right) = \mathbf{n}^T_{\partial\Omega^{(1)}_{1(+\infty)}} \cdot \mathbf{f}^{(1)}\left(\mathbf{x}^{(1)}_1, t_{m\pm}\right) = f^{(1)}\left(\mathbf{x}^{(1)}_1, t_{m\pm}\right) = \ddot{x}^{(1)}_1 = -g,\\
&G^{(1,1)}_{\partial\Omega^{(1)}_{1(+\infty)}}\left(\mathbf{x}^{(1)}_1, t_{m\pm}\right) = \mathbf{n}^T_{\partial\Omega^{(1)}_{1(+\infty)}} \cdot D\mathbf{f}^{(1)}\left(\mathbf{x}^{(1)}_1, t_{m\pm}\right) = \frac{d}{dt} f^{(1)}\left(\mathbf{x}^{(1)}_1, t\right)\Big|_{t=t_{m\pm}} = \dddot{x}^{(1)}_1 = 0\\
&\qquad\qquad \text{for } \partial\Omega^{(1)}_{1(+\infty)} \text{ in the absolute frame,}\\
&G^{(0,1)}_{\partial\Omega^{(i)}_{1(-\infty)}}\left(\mathbf{z}^{(i)}_1, t_{m\pm}\right) = \mathbf{n}^T_{\partial\Omega^{(i)}_{1(-\infty)}} \cdot \mathbf{g}^{(i)}\left(\mathbf{z}^{(i)}_1, \mathbf{x}^{(\bar{i})}_1, t_{m\pm}\right) = g^{(i)}\left(\mathbf{z}^{(i)}_1, \mathbf{x}^{(\bar{i})}_1, t_{m\pm}\right) = \ddot{z}^{(i)}_1\left(t_{m\pm}\right),\\
&G^{(1,1)}_{\partial\Omega^{(i)}_{1(-\infty)}}\left(\mathbf{z}^{(i)}_1, t_{m\pm}\right) = \mathbf{n}^T_{\partial\Omega^{(i)}_{1(-\infty)}} \cdot D\mathbf{g}^{(i)}\left(\mathbf{z}^{(i)}_1, \mathbf{x}^{(\bar{i})}_1, t_{m\pm}\right) = \frac{d}{dt} g^{(i)}\left(\mathbf{z}^{(i)}_1, \mathbf{x}^{(\bar{i})}_1, t\right)\Big|_{t=t_{m\pm}} = \dddot{z}^{(i)}_1\left(t_{m\pm}\right)\\
&\qquad\qquad \text{for } \partial\Omega^{(i)}_{1(-\infty)} \text{ in the relative frame.}
\end{aligned} \tag{3.18}$$

Based on the normal vectors and G-functions, the analytical condition for stick motion is obtained for the condition for a passable flow from domain $\Omega^{(i)}_1$ to $\Omega^{(i)}_0$ in Luo [49] or [50], that is,

$$(-1)^i G^{(0,1)}_{\partial\Omega^{(i)}_{10}}\left(\mathbf{z}^{(i)}_1, t_{m-}\right) > 0, \qquad (-1)^i G^{(0,1)}_{\partial\Omega^{(i)}_{10}}\left(\mathbf{z}^{(i)}_0, t_{m+}\right) > 0. \tag{3.19}$$

Therefore, one obtains

$$(-1)^i g^{(i)}_1\left(\mathbf{z}^{(i)}_1, \mathbf{x}^{(\bar{i})}_1, t_{m-}\right) > 0, \qquad (-1)^i g^{(i)}_0\left(\mathbf{z}^{(i)}_0, \mathbf{x}^{(\bar{i})}_0, t_{m+}\right) > 0. \tag{3.20}$$

With the relative force function per unit mass (i.e., relative acceleration $\ddot{z}^{(i)} = \ddot{x}^{(i)} - \ddot{x}^{(\bar{i})}$), equations of (3.20) gives

$$\ddot{x}^{(2)}\left(t_{m\pm}\right) > \ddot{x}^{(1)}\left(t_{m\pm}\right) = -g. \tag{3.21}$$

From (3.21), the stick motion requires that the acceleration of the piston $\ddot{x}^{(2)}(t_{m\pm})$ is greater than $\ddot{x}^{(1)}(t_{m\pm}) = -g$. In a similar fashion, the condition for vanishing of the stick motion at $\partial\Omega^{(i)}_{01}$ in the relative frame is given by

$$\begin{aligned}
&G^{(0,0)}_{\partial\Omega^{(i)}_{01}}\left(\mathbf{z}^{(i)}_0, t_{m-}\right) = 0, \qquad G^{(0,1)}_{\partial\Omega^{(i)}_{01}}\left(\mathbf{z}^{(i)}_1, t_{m+}\right) = 0,\\
&(-1)^i G^{(1,0)}_{\partial\Omega^{(i)}_{01}}\left(\mathbf{z}^{(i)}_0, t_{m-}\right) < 0, \qquad (-1)^i G^{(1,1)}_{\partial\Omega^{(i)}_{01}}\left(\mathbf{z}^{(i)}_1, t_{m+}\right) < 0.
\end{aligned} \tag{3.22}$$

From equations of (3.22), one obtains the relative force relations or $\partial\Omega_{01}^{(i)}$ as

$$\begin{aligned} g_0^{(i)}\left(\mathbf{z}_0^{(i)}, \mathbf{x}_0^{(\bar{i})}, t_{m-}\right) = 0, \qquad g_1^{(i)}\left(\mathbf{z}_1^{(i)}, \mathbf{x}_1^{(\bar{i})}, t_{m+}\right) = 0, \\ (-1)^i \frac{d}{dt} g_0^{(i)}\left(\mathbf{z}_0^{(i)}, \mathbf{x}_0^{(\bar{i})}, t_{m-}\right) < 0, \qquad (-1)^i \frac{d}{dt} g_1^{(i)}\left(\mathbf{z}_1^{(i)}, \mathbf{x}_1^{(\bar{i})}, t_{m+}\right) < 0. \end{aligned} \tag{3.23}$$

With the relative acceleration ($\ddot{z}^{(i)} = \ddot{x}^{(i)} - \ddot{x}^{(\bar{i})}$) and relative jerk ($\dddot{z}^{(i)} = \dddot{x}^{(i)} - \dddot{x}^{(\bar{i})}$), equations of (3.22) can be rewritten as

$$\ddot{x}^{(2)}\left(t_{m\pm}\right) = \ddot{x}^{(1)}\left(t_{m\pm}\right) = -g, \quad \dddot{x}_{m\pm}^{(2)} < \dddot{x}_{m\pm}^{(1)} = 0 \quad \text{for } \partial\Omega_{01}^{(i)}. \tag{3.24}$$

The stick motion vanishing at the switching boundary requires that the piston's jerk is less than zero as both accelerations are the gravitational acceleration.

Based on the G-functions of a flow to the impacting boundaries, the conditions of grazing motions are also developed, that is,

$$\begin{aligned} G_{\partial\Omega_{1(+\infty)}^{(1)}}^{(0,1)}\left(\mathbf{x}_1^{(1)}, t_{m\pm}\right) = 0, \quad G_{\partial\Omega_{1(+\infty)}^{(1)}}^{(1,1)}\left(\mathbf{x}_1^{(1)}, t_{m\pm}\right) < 0 \quad \text{for } \partial\Omega_{1(+\infty)}^{(i)}, \\ (-1)^i G_{\partial\Omega_{1(-\infty)}^{(1)}}^{(0,1)}\left(\mathbf{z}_1^{(i)}, t_{m\pm}\right) = 0, \quad (-1)^i G_{\partial\Omega_{1(-\infty)}^{(1)}}^{(0,1)}\left(\mathbf{z}_1^{(i)}, t_{m\pm}\right) < 0 \quad \text{for } \partial\Omega_{1(-\infty)}^{(i)}. \end{aligned} \tag{3.25}$$

The grazing conditions for the boundaries of nonstick motions reduce to

$$\begin{aligned} \dot{x}^{(1)} = 0, \quad \ddot{x}^{(1)} = -g < 0 \quad \text{for } \partial\Omega_{1(+\infty)}^{(1)}, \\ \dot{x}^{(1)} = \dot{x}^{(2)}, \quad \ddot{x}^{(2)} < \ddot{x}^{(1)} = -g \quad \text{for } \partial\Omega_{1(-\infty)}^{(i)}. \end{aligned} \tag{3.26}$$

From the first equation of (3.26), the ball grazing at the fixed wall requires that the velocity of ball be zero because the acceleration of ball ($\ddot{x}^{(1)} = -g$) is always zero. However, from the second equation of (3.26), for the ball grazing at the impacting boundary with piston, the piston acceleration should be less than the ball acceleration (i.e., $\ddot{x}^{(1)} = -g$). In other words, this condition is also for the piston motion grazing at this impacting boundary with the ball.

In a similar fashion, the grazing conditions for the boundary of the stick motion are

$$\begin{aligned} G_{\partial\Omega_{10}^{(i)}}^{(0,1)}\left(\mathbf{z}_1^{(i)}, t_{m\pm}\right) = 0, \quad (-1)^i G_{\partial\Omega_{10}^{(i)}}^{(1,1)}\left(\mathbf{z}_1^{(i)}, t_{m\pm}\right) < 0 \quad \text{for } \partial\Omega_{10}^{(i)}, \\ G_{\partial\Omega_{01}^{(i)}}^{(0,0)}\left(\mathbf{z}_0^{(i)}, t_{m\pm}\right) = 0, \quad (-1)^i G_{\partial\Omega_{01}^{(i)}}^{(1,0)}\left(\mathbf{z}_0^{(i)}, t_{m\pm}\right) > 0 \quad \text{for } \partial\Omega_{01}^{(i)}. \end{aligned} \tag{3.27}$$

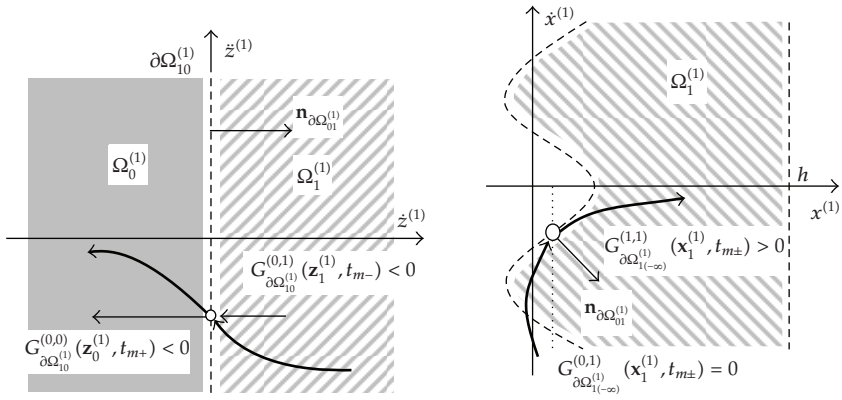

Figure 5: (a) Passable motion and (b) grazing motion.

Again, with the relative acceleration ($\ddot{z}^{(i)} = \ddot{x}^{(i)} - \ddot{x}^{(\bar{i})}$) and relative jerk ($\dddot{z}^{(i)} = \dddot{x}^{(i)} - \dddot{x}^{(\bar{i})}$), the grazing conditions are given by the accelerations and jerks of piston and ball, that is,

$$\begin{aligned} &\ddot{x}^{(2)} = \ddot{x}^{(1)} = -g, \quad \dddot{x}^{(2)} < \dddot{x}^{(1)} = 0 \quad \text{for } \partial\Omega_{10}^{(i)}, \\ &\ddot{x}^{(2)} = \ddot{x}^{(1)} = -g, \quad \dddot{x}^{(2)} > \dddot{x}^{(1)} = 0 \quad \text{for } \partial\Omega_{01}^{(i)}. \end{aligned} \tag{3.28}$$

To geometrically explain the above analytical conditions, consider a flow of the motion approaching the stick boundary $\partial\Omega_{10}^{(1)}$ at $(\mathbf{z}_1^{(1)}, t_{m-})$. In order for such a flow to pass the boundary, the normal vector fields of $G_{\partial\Omega_{10}^{(i)}}^{(0,1)}$ and $G_{\partial\Omega_{01}^{(i)}}^{(0,0)}$ have to point toward the stick domain $\Omega_1^{(i)}$ (i.e., $(-1)^i G_{\partial\Omega_{10}^{(i)}}^{(0,1)} > 0$, $(-1)^i G_{\partial\Omega_{01}^{(i)}}^{(0,0)} > 0$) because the normal vector points to the domain $\Omega_1^{(i)}$. Such conditions are given in (3.19) (or (3.21)) and the flow of motion will pass over the boundary and gets into the stick domain $\Omega_0^{(i)}$. Such a motion is a passable motion to the boundary $\partial\Omega_{10}^{(1)}$, as shown in Figure 5(a). For this case, the stick motion is formed. Similarly, for a flow from a stick domain to the nonstick domain, a flow of motion needs to satisfy the conditions in (3.22) (or (3.23)). Such a passable flow is called the vanishing of stick motion. When a flow of motion approaches the impact chatter boundary $\partial\Omega_{1(-\infty)}^{(1)}$ at $(\mathbf{z}_1^{(1)}, t_{m-})$, if the normal vector field $G_{\partial\Omega_{1(-\infty)}^{(1)}}^{(0,1)}$ be equal to zero and the total change rate of the normal vector field $G_{\partial\Omega_{1(-\infty)}^{(1)}}^{(1,1)}$ is greater than zero in domain $\Omega_1^{(1)}$ (i.e., $G_{\partial\Omega_{1(-\infty)}^{(1)}}^{(0,1)} = 0$ and $G_{\partial\Omega_{1(-\infty)}^{(1)}}^{(1,1)} > 0$), the flow of motion will leave the boundary and stay in domain $\Omega_1^{(1)}$, as sketched in Figure 5(b). Such a motion is called a grazing motion to the boundary $\partial\Omega_{1(-\infty)}^{(1)}$. The corresponding condition for grazing at $\partial\Omega_{1(-\infty)}^{(1)}$ is presented in (3.25). Similarly, for the stick boundary $\partial\Omega_{01}^{(1)}$, the grazing condition in (3.27) can be geometrically explained.

4. Mapping Structures and Motions

In this section, the switching sets and mapping structures will be introduced to symbolically describe motions in the generalized Fermi-acceleration oscillator. The switching sets will be

defined from the switching boundaries. From the switching sets, the generic mappings in domains will be introduced. The mapping structure for periodic and chaotic motions will be constructed from such generic mappings. The stability and bifurcation conditions will also be discussed via the eigenvalue analysis.

4.1. Switching Sets and Generic Mappings

Based on the switching boundaries in (3.2), the switching sets of the generalized Fermi-acceleration oscillator without stick are defined as

$$\begin{aligned}\Sigma_{1(-\infty)} &= \Sigma^{(1)}_{1(-\infty)} \otimes \Sigma^{(2)}_{1(-\infty)} = \left\{ \left(x_i^{(1)}, \dot{x}_i^{(1)}, x_i^{(2)}, \dot{x}_i^{(2)}, t_i \right) \mid x_i^{(1)} = x_{i+}^{(2)}, \dot{x}_i^{(1)} \neq \dot{x}_i^{(2)} \right\}, \\ \Sigma_{1(+\infty)} &= \Sigma^{(1)}_{1(+\infty)} \otimes \Sigma^{(2)}_{1(+\infty)} = \left\{ \left(x_i^{(1)}, \dot{x}_i^{(1)}, x_i^{(2)}, \dot{x}_i^{(2)}, t_i \right) \mid x_i^{(1)} = h, \dot{x}_i^{(1)} \neq 0 \right\},\end{aligned} \tag{4.1}$$

where the symbol $\otimes$ represents the direct product of switching subsets, and the switching subsets ($\Sigma^{(i)}_{1(-\infty)}$ and $\Sigma^{(i)}_{1(+\infty)}$) on the boundaries ($\partial\Omega^{(i)}_{1(-\infty)}$ and $\partial\Omega^{(i)}_{1(+\infty)}$) are defined as

$$\begin{aligned}\Sigma^{(i)}_{1(-\infty)} &= \left\{ \left(x_k^{(i)}, \dot{x}_k^{(i)}, t_k \right) \mid x_k^{(i)} = x_k^{(\bar{i})}, \dot{x}_k^{(i)} \neq \dot{x}_k^{(\bar{i})} \right\} \subset \partial\Omega^{(i)}_{1(-\infty)}, \\ \Sigma^{(i)}_{1(+\infty)} &= \left\{ \left(x_k^{(i)}, \dot{x}_k^{(i)}, t_k \right) \mid x_k^{(1)} = h, \dot{x}_k^{(1)} \neq 0 \right\} \subset \partial\Omega^{(i)}_{1(+\infty)}.\end{aligned} \tag{4.2}$$

Thus, the generic mappings for motions without stick are defined as

$$P_1 : \Sigma_{1(-\infty)} \longrightarrow \Sigma_{1(+\infty)}, \qquad P_2 : \Sigma_{1(+\infty)} \longrightarrow \Sigma_{1(-\infty)}, \qquad P_3 : \Sigma_{1(-\infty)} \longrightarrow \Sigma_{1(-\infty)}, \tag{4.3}$$

where the mappings P_1 and P_2 are the global mappings and the mapping P_3 is a local mapping. No any mapping exists from $\Sigma_{1(+\infty)}$ to $\Sigma_{1(+\infty)}$ because $\ddot{x}^{(1)} = -g$. The global mapping will map one switching set into another one. However, the local mapping will map a switching set into itself. Since the resultant switching set is the direct product of the two switching subsets, a resultant mapping should have two components, that is,

$$\begin{gathered}P_1 = ({}^{(1)}P_1, {}^{(2)}P_1), \qquad P_2 = ({}^{(1)}P_2, {}^{(2)}P_1), \qquad P_3 = ({}^{(1)}P_3, {}^{(2)}P_1), \\ {}^{(i)}P_1 : \Sigma^{(i)}_{1(-\infty)} \longrightarrow \Sigma^{(i)}_{1(+\infty)}, \qquad {}^{(i)}P_2 : \Sigma^{(i)}_{1(+\infty)} \longrightarrow \Sigma^{(i)}_{1(-\infty)}, \qquad {}^{(i)}P_3 : \Sigma^{(i)}_{1(-\infty)} \longrightarrow \Sigma^{(i)}_{1(-\infty)}.\end{gathered} \tag{4.4}$$

From the above definitions, the switching subsets and submappings are sketched in Figures 6(a) and 6(b) for the particle and piston. The switching points in the switching sets are presented by the circular symbols, and the mappings are depicted by the curves with arrows.

Similarly, from the switching boundaries in (3.2) and (3.4), the switching sets of the generalized Fermi-acceleration oscillator with stick are defined as

$$\begin{aligned}\Sigma_{10} &= \Sigma^{(1)}_{10} \otimes \Sigma^{(2)}_{10} = \left\{ \left(x_k^{(1)}, \dot{x}_k^{(1)}, x_k^{(2)}, \dot{x}_k^{(2)}, t_k \right) \mid x_k^{(1)} = x_k^{(2)}, \dot{x}_k^{(1)} = \dot{x}_k^{(2)} \right\}, \\ \Sigma_{1(+\infty)} &= \Sigma^{(1)}_{1(+\infty)} \otimes \Sigma^{(2)}_{1(+\infty)} = \left\{ \left(x_k^{(1)}, \dot{x}_k^{(1)}, x_k^{(2)}, \dot{x}_k^{(2)}, t_k \right) \mid x_k^{(1)} = h, \dot{x}_k^{(1)} \neq 0 \right\},\end{aligned} \tag{4.5}$$

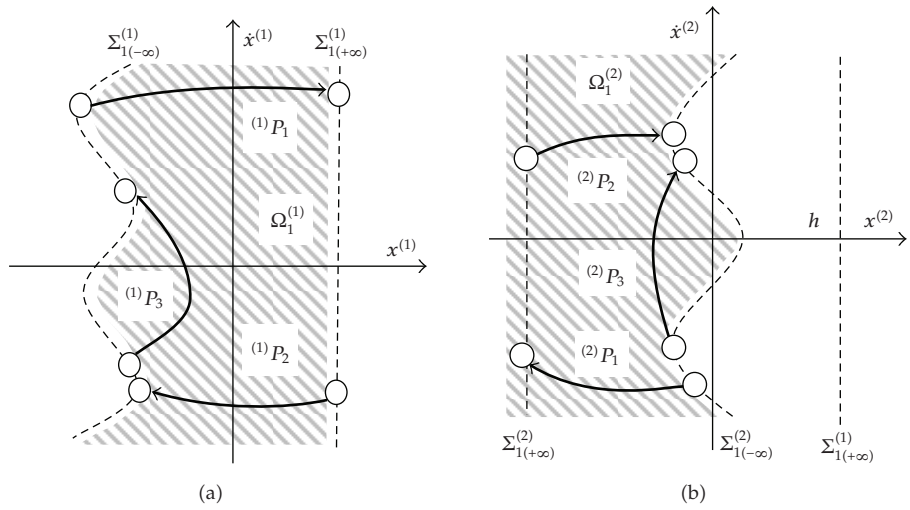

Figure 6: Switching sets and generic mappings for nonstick motion (in absolute coordinates): (a) particle and (b) piston.

where the switching set Σ_{10} is defined on the boundary $\partial\Omega_{10}$

$$\begin{aligned}\Sigma^{(i)}_{10} &= \left\{\left(x^{(i)}_k, \dot{x}^{(i)}_k, t_k\right) \mid x^{(i)}_k = x^{(\bar{i})}_k, \dot{x}^{(i)}_k = \dot{x}^{(\bar{i})}_k\right\} \subset \partial\Omega^{(i)}_{10},\\ \Sigma^{(i)}_{1(+\infty)} &= \left\{\left(x^{(i)}_k, \dot{x}^{(i)}_k, t_k\right) \mid x^{(1)}_k = h, \dot{x}^{(1)}_k \neq 0\right\} \subset \partial\Omega^{(i)}_{1(+\infty)}.\end{aligned} \tag{4.6}$$

Thus, the generic mappings are defined as

$$P_0 : \Sigma_{10} \longrightarrow \Sigma_{10}, \qquad P_1 : \Sigma_{10} \longrightarrow \Sigma_{1(+\infty)}, \qquad P_2 : \Sigma_{1(+\infty)} \longrightarrow \Sigma_{10}, \qquad P_3 : \Sigma_{1(-\infty)} \longrightarrow \Sigma_{10}. \tag{4.7}$$

Similarly, a resultant mapping should have two components, so one obtains

$$\begin{gathered}P_0 = \left(^{(1)}P_0, {}^{(2)}P_0\right), \qquad P_1 = \left(^{(1)}P_1, {}^{(2)}P_1\right), \qquad P_2 = \left(^{(1)}P_2, {}^{(2)}P_2\right), \qquad P_3 = \left(^{(1)}P_3, {}^{(2)}P_3\right),\\ {}^{(i)}P_0 : \Sigma^{(i)}_{10} \longrightarrow \Sigma^{(i)}_{10}, \qquad {}^{(i)}P_1 : \Sigma^{(i)}_{1(-\infty)} \longrightarrow \Sigma^{(i)}_{1(+\infty)},\\ {}^{(i)}P_2 : \Sigma^{(i)}_{1(+\infty)} \longrightarrow \Sigma^{(i)}_{1(-\infty)}, \qquad {}^{(i)}P_3 : \Sigma^{(i)}_{1(-\infty)} \longrightarrow \Sigma^{(i)}_{1(-\infty)},\end{gathered} \tag{4.8}$$

where P_1 and P_2 are the global mappings and P_0 and P_3 are the local mappings. The mappings in (4.8), are sketched in Figure 7.

From the above definitions, a mapping will map a switching set into another switching set (or itself) through the corresponding dynamical system in a specified domain. In such a domain, the dynamical system given in (2.1) or (2.2) is continuous. The solutions for such a continuous system are listed in the appendix. From the displacement and velocity solutions

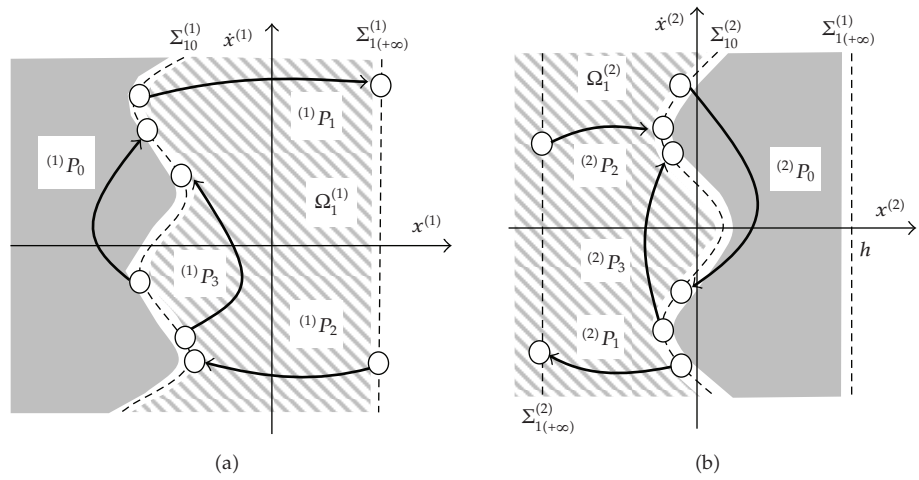

Figure 7: Switching sets and generic mappings for stick motion: (a) particle and (b) piston.

of the particle and piston in the appendix, with switching sets, four algebraic governing equations for a generic mapping P_j $(j = 1, 2, 3)$ can be expressed in a form of

$$P_j : \begin{cases} f_1^{(j)}\left(x_k^{(1)}, \dot{x}_k^{(1)}, x_k^{(2)}, \dot{x}_k^{(2)}, t_k, x_{k+1}^{(1)}, \dot{x}_{k+1}^{(1)}, x_{k+1}^{(2)}, \dot{x}_{k+1}^{(2)}, t_{k+1}\right) = 0, \\ f_2^{(j)}\left(x_k^{(1)}, \dot{x}_k^{(1)}, x_k^{(2)}, \dot{x}_k^{(2)}, t_k, x_{k+1}^{(1)}, \dot{x}_{k+1}^{(1)}, x_{k+1}^{(2)}, \dot{x}_{k+1}^{(2)}, t_{k+1}\right) = 0, \\ f_3^{(j)}\left(x_k^{(1)}, \dot{x}_k^{(1)}, x_k^{(2)}, \dot{x}_k^{(2)}, t_k, x_{k+1}^{(1)}, \dot{x}_{k+1}^{(1)}, x_{k+1}^{(2)}, \dot{x}_{k+1}^{(2)}, t_{k+1}\right) = 0, \\ f_4^{(j)}\left(x_k^{(1)}, \dot{x}_k^{(1)}, x_k^{(2)}, \dot{x}_k^{(2)}, t_k, x_{k+1}^{(1)}, \dot{x}_{k+1}^{(1)}, x_{k+1}^{(2)}, \dot{x}_{k+1}^{(2)}, t_{k+1}\right) = 0, \end{cases} \tag{4.9}$$

with

$$\begin{aligned} &x_k^{(1)} = h, \quad x_{k+1}^{(1)} = x_{k+1}^{(2)} \quad \text{for } P_1, \\ &x_k^{(1)} = x_k^{(2)}, \quad x_{k+1}^{(1)} = h \quad \text{for } P_2, \\ &x_k^{(1)} = x_k^{(1)}, \quad x_{k+1}^{(1)} = x_{k+1}^{(2)} \quad \text{for } P_3. \end{aligned} \tag{4.10}$$

The governing equations for the stick mapping P_0 can be expressed by

$$P_0 : \begin{cases} f_1^{(0)}\left(x_k^{(i)}, \dot{x}_k^{(i)}, t_k, x_{k+1}^{(i)}, \dot{x}_{k+1}^{(i)}, t_{k+1}\right) = 0, \\ f_2^{(0)}\left(x_k^{(i)}, \dot{x}_k^{(i)}, t_k, x_{k+1}^{(i)}, \dot{x}_{k+1}^{(i)}, t_{k+1}\right) = 0, \\ f_4^{(0)}\left(x_{k+1}^{(i)}, \dot{x}_{k+1}^{(i)}, t_{k+1}\right) = g_1^{(i)}\left(0, \mathbf{x}_{k+1}^{(i)}, t_{k+1}\right) = 0, \end{cases} \tag{4.11}$$

with

$$\begin{aligned} x_k^{(i)} &= x_k^{(\bar{i})}, \quad \dot{x}_k^{(i)} = \dot{x}_k^{(\bar{i})}, \\ x_{k+1}^{(i)} &= x_{k+1}^{(\bar{i})}, \quad \dot{x}_{k+1}^{(i)} = \dot{x}_{k+1}^{(\bar{i})}, \quad \text{for mapping } P_0. \\ \ddot{x}_k^{(2)} &> -g, \quad \ddot{x}_{k+1}^{(2)} < -g, \end{aligned} \tag{4.12}$$

4.2. Motions with Mapping Structures

The notation for mapping action is introduced as

$$P_{j_k j_{k-1} \cdots j_1} = P_{j_k} \circ P_{j_{k-1}} \circ \cdots \circ P_{j_1}, \tag{4.13}$$

where $j_m \in \{0,1,2,3\}$ with $m = 1,2,\ldots,k$. For a motion with n-time repeats of mapping structure of $P_{j_1 j_2 \cdots j_k}$, the mapping structure is expressed as

$$P_{j_k j_{k-1} \cdots j_1}^{(m)} = \underbrace{\left(P_{j_k} \circ P_{j_{k-1}} \circ \cdots \circ P_{j_1}\right) \circ \cdots \circ \left(P_{j_k} \circ P_{j_{k-1}} \circ \cdots \circ P_{j_1}\right)}_{n} = P_{(j_k j_{k-1} \cdots j_1)^n}. \tag{4.14}$$

Any periodic motion can be described using the above notations. Consider a mapping structure for the generalized Fermi-acceleration oscillator as

$$P = P_{3^n} \circ P_{0^{k_3}} \circ P_{3^m} \circ P_{2^{k_2}} \circ P_{1^{k_1}} = P_{3^n 0^{k_3} 3^m 2^{k_2} 1^{k_1}}, \tag{4.15}$$

where $k_j \in \{0,1\}$ and $m,n \in \{0,\mathbb{N}\}$. From the mapping of (4.15), a periodic motion can be expressed. By period-doubling, the corresponding mapping structures for motion relative to the foregoing mapping structure $P_{3^n 0^{k_3} 3^m 2^{k_2} 1^{k_1}}$ of (4.15) are

$$\begin{aligned} P &= P_{3^n 0^{k_3} 3^m 2^{k_2} 1^{k_1}} \circ P_{3^n 0^{k_3} 3^m 2^{k_2} 1^{k_1}} = P_{(3^n 0^{k_3} 3^m 2^{k_2} 1^{k_1})^2}, \\ &\vdots \\ P &= P_{(3^n 0^{k_3} 3^m 2^{k_2} 1^{k_1})^{2^{l-1}}} \circ P_{(3^n 0^{k_3} 3^m 2^{k_2} 1^{k_1})^{2^{l-1}}} = P_{(3^n 0^{k_3} 3^m 2^{k_2} 1^{k_1})^{2^l}}. \end{aligned} \tag{4.16}$$

For $l \to \infty$, the chaotic motion relative to $P_{3^n 0^{k_3} 3^m 2^{k_2} 1^{k_1}}$ can be obtained.

Once the grazing bifurcation of the periodic motion of $P_{3^n 0^{k_3} 3^m 2^{k_2} 1^{k_1}}$ occurs, the corresponding mapping structure will change dramatically. For instance, the changed mapping structure can be expressed by two parts of mapping structures, that is,

$$\begin{aligned} P &= P_{3^{n_2} 0^{k_{32}} 3^{m_2} 2^{k_{22}} 1^{k_{12}}} \circ P_{3^{n_1} 0^{k_{31}} 3^{m_1} 2^{k_{21}} 1^{k_{11}}} \\ &= P_{(3^{n_2} 0^{k_{32}} 3^{m_2} 2^{k_{22}} 1^{k_{12}})(3^{n_1} 0^{k_{31}} 3^{m_1} 2^{k_{21}} 1^{k_{11}})}, \end{aligned} \tag{4.17}$$

where $k_{js} \in \{0,1\}$ and $m_s, n_s \in \mathbb{N}$ $(s = 1,2)$. For a generalized case, the mapping structure is

$$P = \underbrace{P_{3^{n_l}0^{k_{3l}}3^{m_l}2^{k_{2l}}1^{k_{1l}}} \circ \cdots \circ P_{3^{n_1}0^{k_{31}}3^{m_1}2^{k_{21}}1^{k_{11}}}}_{l\text{-terms}} = P_{\underbrace{(3^{n_l}0^{k_{3l}}3^{m_l}2^{k_{2l}}1^{k_{1l}})\cdots(3^{n_1}0^{k_{31}}3^{m_1}2^{k_{21}}1^{k_{11}})}_{l\text{-terms}}}, \tag{4.18}$$

where $k_{js} \in \{0,1\}$ and $m_s, n_s \in \mathbb{N}$ $(s = 1,2,\ldots,l)$. Such mapping structure can be used to express all possible motions in the generalized Fermi-acceleration oscillator. In addition, the grazing bifurcation of chaotic motions will cause the strange attractor fragmentation (see Luo [41]).

Without stick, there are two types of motions: (i) impact only at the boundary $\partial\Omega_{1(-\infty)}$ and (ii) impacts at both of the boundaries $\partial\Omega_{1(-\infty)}$ and $\partial\Omega_{1(+\infty)}$. For the first case, the motion interacts with the boundary $\partial\Omega_{1(-\infty)}$ ($k_{1s} = 0$, $k_{2s} = 0$, and $k_{3s} = 0$, $s \in \mathbb{N}$) only. This motion can be described by the generic mapping P_3. The motion pattern relative to P_{3^m}, caused by the period-doubling bifurcation, is given by

$$\begin{aligned} &P = P_{3^m}, \\ &P = P_{3^m} \circ P_{3^m} = P_{3^{2m}}, \\ &\vdots \\ &P = P_{3^{2^{l-1}m}} \circ P_{3^{2^{l-1}m}} = P_{3^{2^l m}}. \end{aligned} \tag{4.19}$$

The motion pattern relative to P_{3^m} can be generated by the grazing bifurcation, and the corresponding mapping structures are

$$\begin{aligned} &P = P_{3^m}, \\ &P = P_{3^{m_1}} \circ P_3 \circ P_{3^{m_2}} = P_{3^{m+1}}, \\ &\vdots \\ &P = P_{3^m} \circ P_{3^n} = P_{3^{m+n}}. \end{aligned} \tag{4.20}$$

The second case is that the motion interacts with boundaries $\partial\Omega_{1(-\infty)}$ and $\partial\Omega_{1(+\infty)}$ ($k_{3s} = 0$, $s \in \mathbb{N}$, $m, n \in \{0, \mathbb{N}\}$). Consider a mapping structure of $P_{3^m 2^{k_2} 1^{k_1}}$. The motion pattern generated by the period-doubling is expressed by

$$\begin{aligned} &P = P_{3^m 2^{k_2} 1^{k_1}} \circ P_{3^m 2^{k_2} 1^{k_1}} = P_{(3^m 2^{k_2} 1^{k_1})^2}, \ldots, \\ &P = P_{(3^m 2^{k_2} 1^{k_1})^{2^{l-1}}} \circ P_{(3^m 2^{k_2} 1^{k_1})^{2^{l-1}}} = P_{(3^m 2^{k_2} 1^{k_1})^{2^l}}. \end{aligned} \tag{4.21}$$

Similarly, the motion pattern generated by the grazing bifurcation can be discussed. To illustrate such mapping structures, the relation between the mappings and motions in phase plane are sketched in Figure 8. The mappings and motions for the piston can be similarly presented. A motion pertaining to mapping $P_{3^m 21}$ is sketched in Figure 8(a). In such a motion, no any stick motions exists. However, a motion with stick is associated with mapping $P_{3^n 03^m 21}$ in Figure 8(b). The mappings are depicted through thick curves, and the impacts are represented by the thin arrows. The stick motion is in the shaded area with mapping P_0. In a similar fashion, any motion with a specific mapping structure can be illustrated.

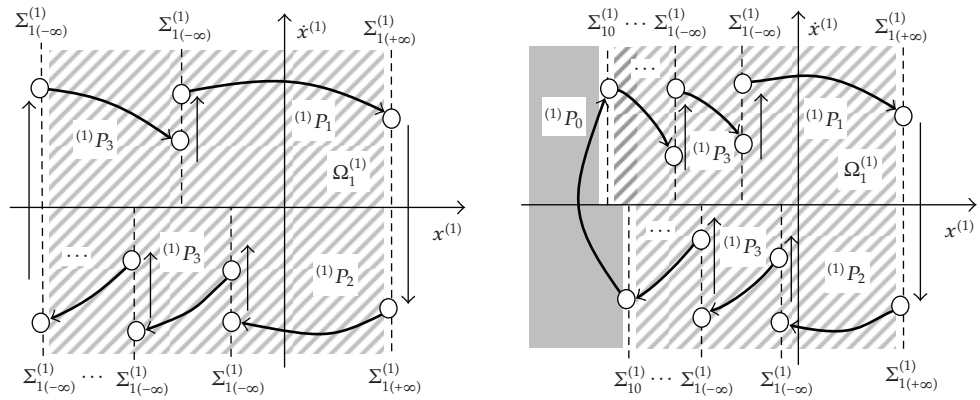

Figure 8: Mapping structure for motions: (a) P_{13^m2} and (b) $P_{13^n03^m2}$.

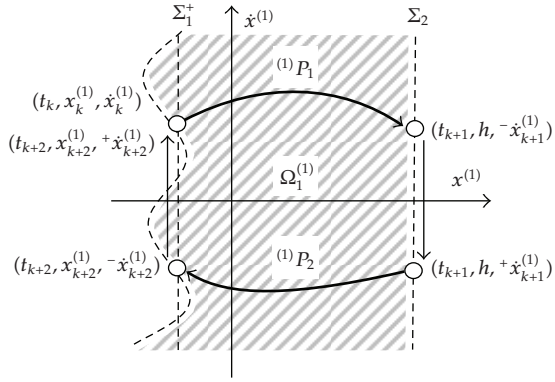

Figure 9: The mapping structure of a simple periodic motion of P_{21}.

4.3. Periodic Motions and Local Stability

Consider a map P_j $(j = 0, 1, 2, 3)$ mapping from the initial state $(x^{(1)}_k, \dot{x}^{(1)}_k, x^{(2)}_k, \dot{x}^{(2)}_k, t_k)$ to the final state $(x^{(1)}_{k+1}, \dot{x}^{(1)}_{k+1}, x^{(2)}_{k+1}, \dot{x}^{(2)}_{k+1}, t_{k+1})$:

$$P_j : \left(x^{(1)}_k, \dot{x}^{(1)}_k, x^{(2)}_k, \dot{x}^{(2)}_k, t_k\right) \longrightarrow \left(x^{(1)}_{k+1}, \dot{x}^{(1)}_{k+1}, x^{(2)}_{k+1}, \dot{x}^{(2)}_{k+1}, t_{k+1}\right). \tag{4.22}$$

From (4.9), the mapping in (4.22) gives four algebraic equations. With boundary constraints, the five variables for the final state can be determined. Without loss of generality, substitution of the boundary constraint into the four algebraic governing equations for P_j $(j = 0, 1, 2, 3)$ yields

$$\mathbf{f}^{(j)}\left(\mathbf{X}_k, \mathbf{Y}_{k+1}\right) = 0, \tag{4.23}$$

where $\mathbf{X}_k = (X_{k1}, X_{k2}, X_{k3}, X_{k4})^T$ with $X_{kr} \in \{x_k^{(1)}, \dot{x}_k^{(1)}, x_k^{(2)}, \dot{x}_k^{(2)}, t_k\}$ and $\mathbf{Y}_k = (Y_{k1}, Y_{k2}, Y_{k3}, Y_{k4})^T$ with $Y_{kr} \in \{x_k^{(1)}, \dot{x}_k^{(1)}, x_k^{(2)}, \dot{x}_k^{(2)}, t_k\}$ and $\mathbf{f}^{(j)} = (f_1^{(j)}, f_2^{(j)}, f_3^{(j)}, f_4^{(j)})^T$. Taking the total derivative of (4.23) with respect to $\mathbf{X}_k$ leads to

$$\begin{gathered}\left[\frac{\partial \mathbf{f}^{(j)}}{\partial \mathbf{X}_k}\right] + \left[\frac{\partial \mathbf{f}^{(j)}}{\partial \mathbf{Y}_{k+1}}\right]\left[\frac{\partial \mathbf{Y}_{k+1}}{\partial \mathbf{X}_k}\right] = 0 \quad \text{or} \\ \frac{\partial f_I^{(j)}}{\partial X_{kJ}} + \sum_{R=1}^{4} \frac{\partial f_I^{(j)}}{\partial Y_{(k+1)R}} \frac{\partial Y_{(k+1)R}}{\partial X_{kJ}} = 0 \quad \text{for } I, J = 1, 2, 3, 4.\end{gathered} \tag{4.24}$$

From the equation of (4.24), one obtains

$$DP_j = \left[\frac{\partial \mathbf{Y}_{k+1}}{\partial \mathbf{X}_k}\right] = -\left[\frac{\partial \mathbf{f}^{(j)}}{\partial \mathbf{Y}_{k+1}}\right]^{-1}\left[\frac{\partial \mathbf{f}^{(j)}}{\partial \mathbf{X}_k}\right], \tag{4.25}$$

where

$$\begin{gathered}\left[\frac{\partial \mathbf{f}^{(j)}}{\partial \mathbf{Y}_{k+1}}\right] = \left[\frac{\partial f_I^{(j)}}{\partial Y_{(k+1)J}}\right]_{4\times 4} \quad \text{for } I, J = 1, 2, 3, 4; \\ \left[\frac{\partial \mathbf{f}^{(j)}}{\partial \mathbf{X}_k}\right] = \left[\frac{\partial f_I^{(j)}}{\partial X_{kJ}}\right]_{4\times 4} \quad \text{for } I, J = 1, 2, 3, 4; \\ DP_j = \left[\frac{\partial \mathbf{Y}_{k+1}}{\partial \mathbf{X}_k}\right] = \left[\frac{\partial Y_{(k+1)I}}{\partial X_{kJ}}\right]_{4\times 4} \quad \text{for } I, J = 1, 2, 3, 4.\end{gathered} \tag{4.26}$$

Consider a simple periodic motion of the mapping structure of $P_{21} = P_2 \circ P_1$ as an example, sketched in Figure 9. With the mapping structure $P_{21} = P_2 \circ P_1$, one obtains

$$\begin{gathered}P_1 : \left(t_k, x_k^{(2)}, \dot{x}_k^{(1)}, \dot{x}_k^{(2)}\right) \longrightarrow \left(t_{k+1}, x_{k+1}^{(2)}, \dot{x}_{k+1}^{(1)}, \dot{x}_{k+1}^{(2)}\right), \\ P_2 : \left(t_{k+1}, x_{k+1}^{(2)}, \dot{x}_{k+1}^{(1)}, \dot{x}_{k+1}^{(2)}\right) \longrightarrow \left(t_{k+2}, x_{k+2}^{(2)}, \dot{x}_{k+2}^{(1)}, \dot{x}_{k+2}^{(2)}\right).\end{gathered} \tag{4.27}$$

Let $X_{k1} = x_k^{(2)} = x_k^{(1)}$, $X_{k2} = \dot{x}_k^{(1)}$, $X_{k3} = \dot{x}_k^{(2)}$, $X_{k4} = t_k$ because the impact occurs at $x_k^{(1)} = x_k^{(2)}$. However, $Y_{k1} = x_k^{(2)}$, $Y_{k2} = \dot{x}_k^{(1)}$, $Y_{k3} = \dot{x}_k^{(2)}$, $Y_{k4} = t_k$ because the impact occurs at $x_k^{(1)} = h$. The corresponding governing equations for such a periodic motion are

$$\begin{gathered}\mathbf{f}^{(1)}\left(\mathbf{X}_k, \mathbf{Y}_{k+1}\right) = 0 \quad \text{for } P_1, \\ \mathbf{f}^{(2)}\left(\mathbf{Y}_{k+1}, \mathbf{X}_{k+2}\right) = 0 \quad \text{for } P_2.\end{gathered} \tag{4.28}$$

For a period-N motion, the periodicity requires

$$\mathbf{X}_k^* = \mathbf{X}_{k+2}^*, \tag{4.29}$$

or

$$\begin{aligned} x_{k+2}^{*(i)} &= x_k^{*(i)}, \quad \dot{x}_{k+2}^{*(i)} = \dot{x}_k^{*(i)}, \\ t_{k+2}^* &= t_k^* + \frac{2N\pi}{\Omega}, \quad N = 1, 2, \ldots, \end{aligned} \qquad \text{for } i = 1, 2. \tag{4.30}$$

Solving (4.28) and (4.29) produces the switching sets of the periodic motion. The Jacobian matrix for each mapping is developed from (4.28) for $j = 1, 2$

$$DP_j = \left[\frac{\partial\left(t_{k+j}, x_{k+j}^{(2)}, \dot{x}_{k+j}^{(1)}, \dot{x}_{k+j}^{(2)}\right)}{\partial\left(t_{k+j-1}, x_{k+j-1}^{(2)}, \dot{x}_{k+j-1}^{(1)}, \dot{x}_{k+j-1}^{(2)}\right)} \right]_{4\times 4}. \tag{4.31}$$

The total Jacobian matrix of the periodic motion can be computed by

$$DP = DP_2 \cdot DP_1. \tag{4.32}$$

The Jacobian matrix of a periodic motion with a generalized mapping structure can be developed in a similar fashion. For a stable periodic motion, the magnitudes of all the eigenvalues should be inside a unit circle, that is,

$$|\lambda_i| < 1, \quad (i = 1, 2, 3, 4). \tag{4.33}$$

If (4.33) cannot be satisfied, then the periodic motion is unstable. Consider a pair of complex eigenvalues ($\lambda_{1,2}$) and the others ($\lambda_{3,4}$). If $|\lambda_{1,2}| = 1$ and $|\lambda_{3,4}| < 1$, the Neirmark bifurcation of the periodic motion takes place. Consider two real eigenvalues ($\lambda_{1,2}$) and the others ($\lambda_{3,4}$). If $\lambda_1 = -1$ and $|\lambda_{2,3,4}| < 1$, the period doubling bifurcation of the periodic motion occurs. If $\lambda_1 = 1$ and $|\lambda_{2,3,4}| < 1$, the saddle-node bifurcation of the periodic motion occurs. However, the eigenvalue analysis cannot be used to predict stick motion and grazing bifurcation. Both of them should be determined through the normal vector fields, and the stick motion is determined by (3.19) and the grazing bifurcation is determined by (3.25).

5. Predictions and Simulations

In this section, bifurcation scenario for the generalized Fermi-acceleration oscillator will be presented first, and analytical predictions of periodic motions will be completed through the mapping structures. Periodic and chaotic motions will be presented for illustration of the analytical conditions. Poincare mapping sections will be given for illustrations of chaotic motions in the Fermi-acceleration oscillator. The parameter maps for certain parameters will also be presented for an overview of dynamical behaviors of particle and piston in the generalized Fermi-acceleration oscillator.

5.1. Bifurcation Scenario

To obtain a bifurcation scenario in the generalized Fermi-acceleration oscillator, the closed-form solutions of particle and piston in the appendix are used for numerical simulations. To achieve a motion with stick, the stick conditions in (3.21) (or $\ddot{x}_k^{(2)} > -g$) with $x_k^{(1)} = x_k^{(2)}$ and $\dot{x}_k^{(1)} = \dot{x}_k^{(2)}$ should be embedded in the computer program. Before stick, the particle and piston are separated. One should set a tolerance of the velocity difference (i.e., $|\dot{x}_k^{(1)} - \dot{x}_k^{(2)}| < \varepsilon$). In computation, the tolerance $\varepsilon < 10^{-4}$ is used for the stick motion. In other words, when $|\dot{x}_k^{(1)} - \dot{x}_k^{(2)}| < 10^{-4}$, it was assumed $\dot{x}_k^{(1)} \approx \dot{x}_k^{(2)}$. If $\ddot{x}_k^{(2)} > -g$, the stick motion of particle and piston is formed, and the two separated dynamical systems in (2.1) will be switched into one dynamical system in (2.2) for the stick motion. Further, the solution of the stick motion in the appendix will be employed for numerical simulations. For the vanishing of the stick motion, the condition in (3.24) (i.e., $\ddot{x}^{(2)}(t_{m\pm}) = \ddot{x}^{(1)}(t_{m\pm}) = -g$ and $\dddot{x}_{m\pm}^{(2)} < \dddot{x}_{m\pm}^{(1)} = 0$) will also be embedded in the computer program. Once the stick motion disappears, the system in (2.2) will become two separated dynamical systems for particle and piston in (2.1). Similarly, the grazing conditions in (3.26) and (3.28) at the corresponding boundaries were embedded in the computer program. The switching points for the particle and piston with switching times are recorded for bifurcation scenarios.

Consider a set of parameters ($m_1 = 0.01$, $m_2 = 1$, $k = 10$, $c = 6$, $e_1 = 0.9$, $e_2 = 0.7$, $h = 1$, $Q = 0.5$). Switching points on the boundaries versus excitation frequency in a bifurcation scenario are shown in Figure 10. The acronyms PD, SN, and GB denote the period-doubling, saddle node, and grazing bifurcations, respectively. In Figure 10(a), the switching displacement of particle versus excitation frequency is presented. The corresponding bifurcations are marked by dashed vertical lines and labeled by the corresponding acronyms (i.e., PD, SN, and GB). The switching displacements for particle impacts for $x^{(1)} = h$ lie on a straight line. However, the switching displacement for the particle impacting with the piston will be changed. The region for the stick motion is labeled. It is observed that the stick motion occurs at the low excitation frequency. Many windows of periodic motions are also observed. The first obvious window of periodic motions is relative to mapping P_{21} for $\Omega \in (21.2, 35.1)$ with one excitation period ($1T$). However, the second obvious window of periodic motions is relative to mapping P_{21} for $\Omega \in (59.3, 70.2)$ with two excitation periods ($2T$). In Figure 10(b), shown are the switching velocities of particle before impact. So the upper branch of the switching velocity of particle is relative to impacts at the fixed wall, and the lower branch of the switching velocity shows the impacts between the particle and piston. In Figure 10(c), the switching displacements of piston are plotted. The switching displacements of impacts and stick between the piston and particle are the same, which are presented by the lower branch of switching displacement. The upper branch of the switching displacement of piston is to record the displacement of piston at impacts between the particle and the fixed wall. Before and after such impacts, the corresponding switching velocity of the piston will not be changed. Therefore, the switching velocities of piston before impacts are plotted in Figure 10(d). In addition, switching times for switching points are very important. Thus, switching phases pertaining to the switching times are plotted in Figure 10(e). From the bifurcation scenario, the motion of P_{21} lies in the range of $\Omega \in (21.2, 35.1)$ and $\Omega \in (59.3, 70.2)$. The motion of $P_{(21)^2}$ lies in the range of $\Omega \in (19.4, 21.2)$ and $\Omega \in (56.8, 59.3)$. The motion of $P_{(21)^4}$ is in the range of $\Omega \in (19.1, 19.4)$ and $\Omega \in (56.4, 56.8)$. In the region of $\Omega \in (0, 19.1)$, the zone of complex motions exists, and in the region of $\Omega \in (35.1, 56.4)$ and $\Omega \in (70.2, 80)$,the

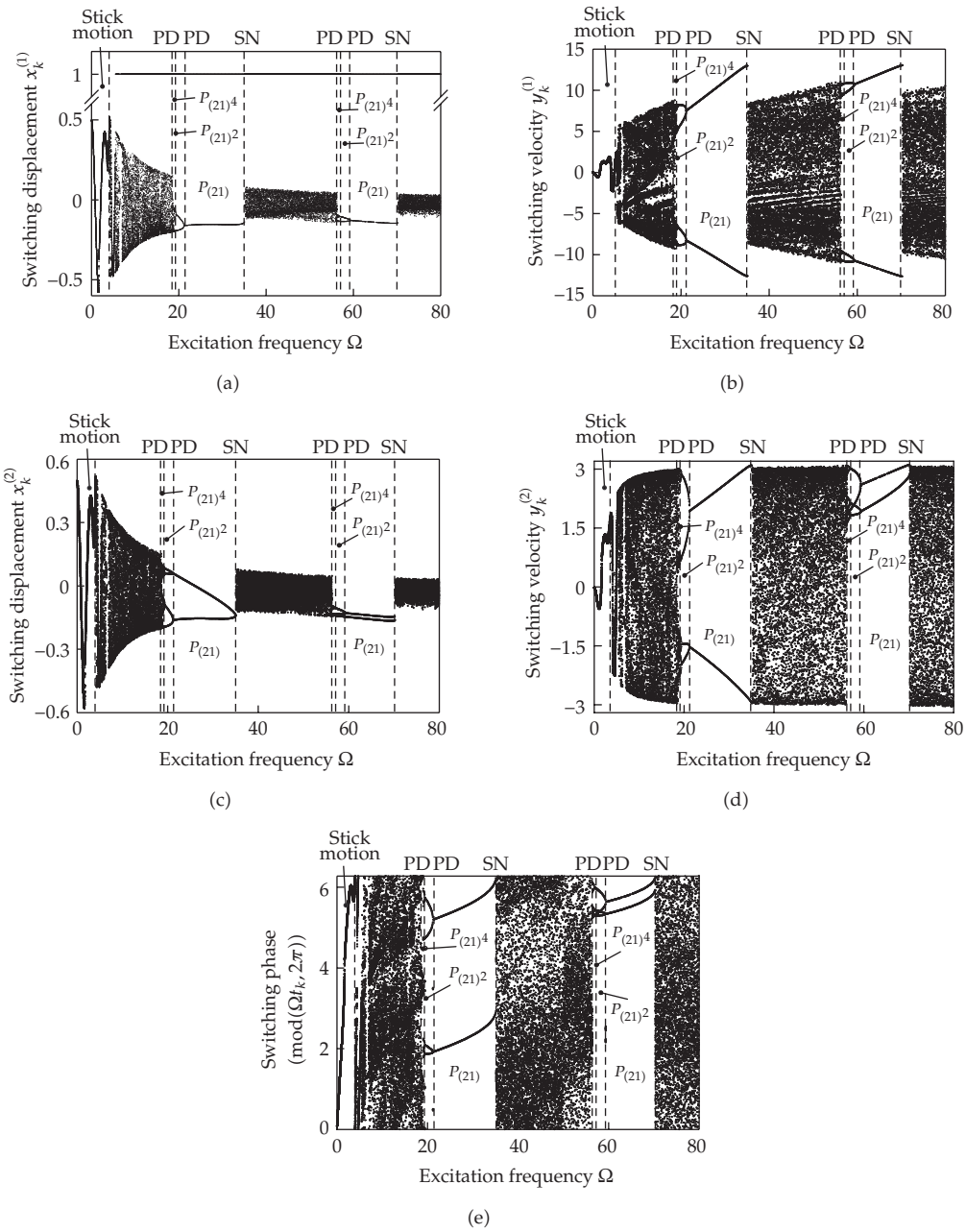

Figure 10: Bifurcation scenario varying with driving frequency: (a) switching displacement and (b) switching velocity of the particle; (c) switching displacement and (d) switching velocity of the piston; (e) Switching phase ($m_1 = 0.01,\ m_2 = 1,\ k = 10,\ c = 6,\ e_1 = 0.9,\ e_2 = 0.7,\ h = 1,\ Q = 0.5$).

zone of chaos exists. In the zone of complex motion, the majority of motions are observable periodic motions with complicated mapping structure. In the zone of chaos, the majority of motions is chaotic. Inside the range of $\Omega \in (0, 6.3)$ there are some simple stick motions. The detailed mapping structures for periodic motions are tabulated in Table 1.

Table 1: Summary of driving frequency for periodic motions ($m_1 = 0.01, m_2 = 1, k = 10, c = 6, e_1 = 0.9, e_2 = 0.7, h = 1, Q = 0.5$).

	Mapping Structure		Excitation Frequency		Mapping Structure		Excitation Frequency
1	$P_{(321)^2}$	P($2T$)	(6.33, 6.56)	16	$P_{(32121)^2}$	P($4T$)	(11.01, 11.05) (11.35, 11.40)
2	P_{321}	P(T)	(6.56, 7.01)	17	P_{32121}	P($2T$)	(11.05, 11.16) (11.40, 11.52)
3	$P_{(333321)^2}$	P($2T$)	(7.41, 7.43)	18	$P_{(321)^4}$	P($8T$)	(11.75, 11.76)
4	$P_{3(321)^2}$	P($3T$)	(7.60, 7.80) (7.91, 7.93)	19	$P_{(321)^2}$	P($4T$)	(11.76, 11.77)
5	$P_{(33(321)^2)^2}$	P($6T$)	(7.87, 7.89)	20	P_{3^2}	P($4T$)	(11.77, 11.79)
6	$P_{33(321)^2}$	P($3T$)	(8.05, 8.07) (8.18, 8.20)	21	P_{3^4}	P($8T$)	(11.79, 11.80)
7	$P_{3(3(321)^2)^2}$	P($6T$)	(8.27, 8.29)	22	$P_{(21)^4}$	P($4T$)	(19.15, 19.40)
8	$P_{(33321)^2}$	P($6T$)	(8.62, 8.64)	23	$P_{(21)^2}$	P($2T$)	(19.40, 21.25)
9	$P_{(3(3321)^2)^2}$	P($8T$)	(8.76, 8.78)	24	P_{21}	P(T)	(21.25, 35.20)
10	$P_{3(3321)^2}$	P($4T$)	(8.94, 8.96)	25	$P_{(21)^4}$	P($8T$)	(56.42, 56.92)
11	$P_{(3321)^4}$	P($8T$)	(9.06, 9.07)	26	$P_{(21)^2}$	P($4T$)	(56.92, 59.35)
12	$P_{(3321)^2}$	P($4T$)	(9.07, 9.09) (9.81, 9.83)	27	P_{21}	P($2T$)	(59.35, 70.23)
14	$P_{(321)^2 33(21)^2}$	P($6T$)	(10.42, 10.44)	28	Chaos & Complex Motion	—	(7.01, 19.15) (19.15, 35.20) (70.23, 80.00)
15	$P_{(32121)^4}$	P($8T$)	(11.00, 11.01) (11.34, 11.35)				

5.2. Analytical Prediction

The analytical prediction of periodic motions is based on the corresponding mapping structures presented in Section 4 to solve the switching points of the periodic motions. In other words, for a specified mapping structure, a set of nonlinear algebraic equations can be developed, and such nonlinear algebraic equations are solved by the Newton-Raphson method to obtain the switching points. The local stability and bifurcation analysis of the periodic motion are also completed as presented in Section 4.2. In this section, the analytical prediction of periodic motions will be presented via two examples, and the corresponding eigenvalue analysis will be given.

Consider $m_1 = 0.01$, $m_2 = 1$, $k = 10$, $c = 6$, $e_1 = 0.9$, $e_2 = 0.7$, $h = 1$, $Q = 0.5$. The analytical prediction of the periodic motions pertaining to mapping $P_{(21)^k}$ ($k = 1, 2, 2^2 \cdots$) is presented in Figure 11, and the corresponding eigenvalues of the periodic motions are shown in Figure 12. The solid curves represent stable solutions, which can be observed in the bifurcation scenario. The dashed curves denote unstable solutions that may exist in the region of chaotic motion in the bifurcation scenario. The acronyms PD, SN, and GB represent the period-doubling, saddle-node, and grazing bifurcations, respectively. From this analytical prediction of periodic motions, the stable solution disappears at the saddle-node bifurcation with $\Omega = 35.20$. The unstable solution of mapping structure P_{21} disappears at the grazing bifurcation with $\Omega = 5.88$. The unstable solutions of mapping structure $P_{(21)^2}$ and $P_{(21)^4}$ vanish at the grazing bifurcations with $\Omega = 9.39$. The saddle-node bifurcation of the periodic motion

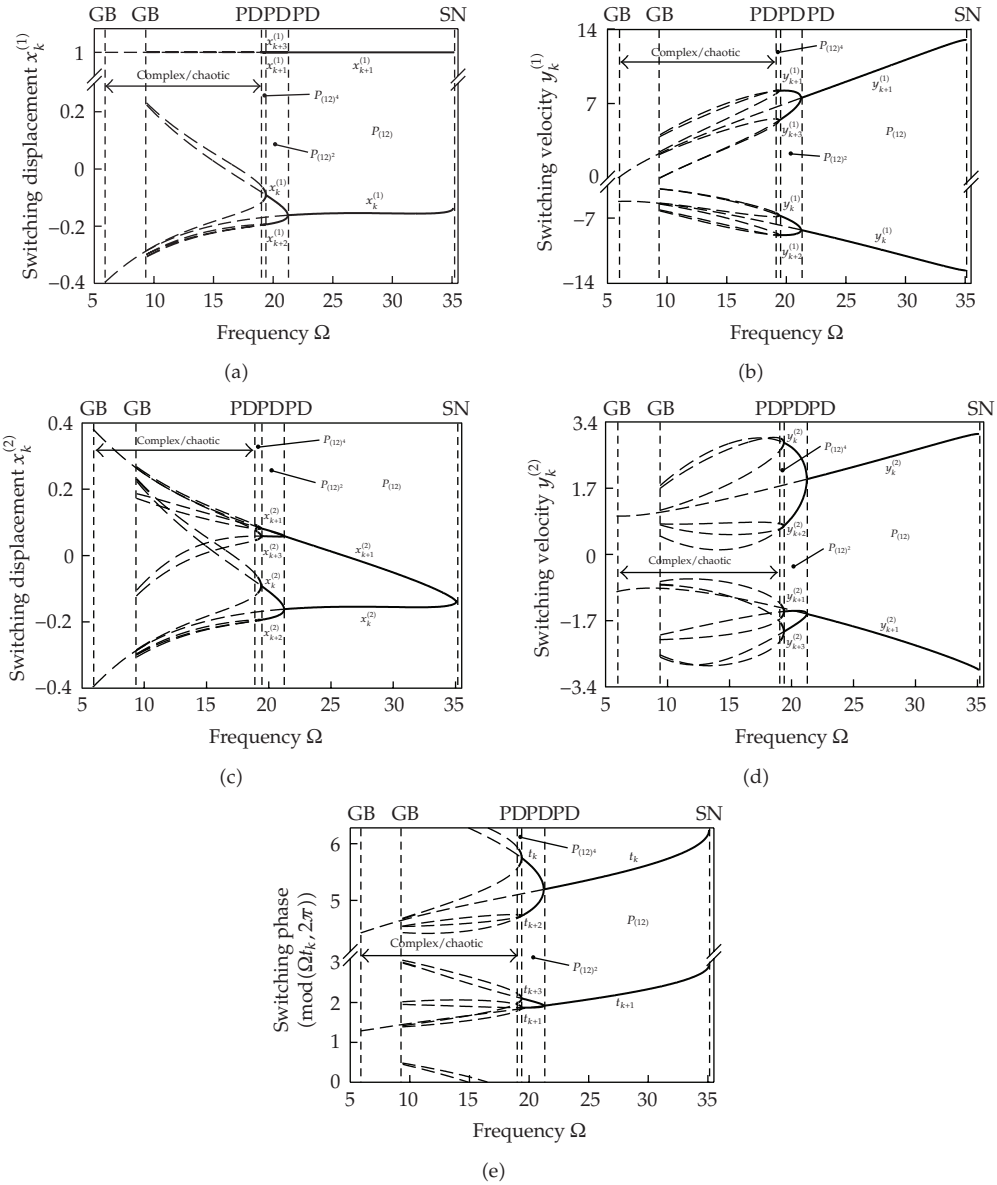

Figure 11: Analytical prediction of periodic motion for $\Omega \in (21, 35)$: (a) switching displacement and (b) switching velocity of the particle; (c) switching displacement and (d) switching velocity of the piston; (e) switching phase. Solid and dashed curves represent the stable and unstable solutions, respectively, ($m_1 = 0.01$, $m_2 = 1$, $k = 10$, $c = 6$, $e_1 = 0.9$, $e_2 = 0.7$, $h = 1$, $Q = 0.5$.)

of P_{21} occurs at $\Omega = 35.20$. This is because one of the eigenvalues equals 1 and all the others are inside a unit circle, as shown in Figure 12. At $\Omega = 19.1, 19.4,$ and 21.2, one of the eigenvalues is equal to -1 and all the others are inside a unit circle, and the period-doubling bifurcations of the corresponding motion of $P_{(21)^4}$, $P_{(21)^2}$, and P_{21} occur. At $\Omega = 5.88$ and 9.39, the grazing bifurcations of periodic motions of P_{21} and ($P_{(21)^4}$, $P_{(21)^2}$) occur, and such periodic motions are unstable. Such a grazing bifurcation should be determined from the normal vector fields and

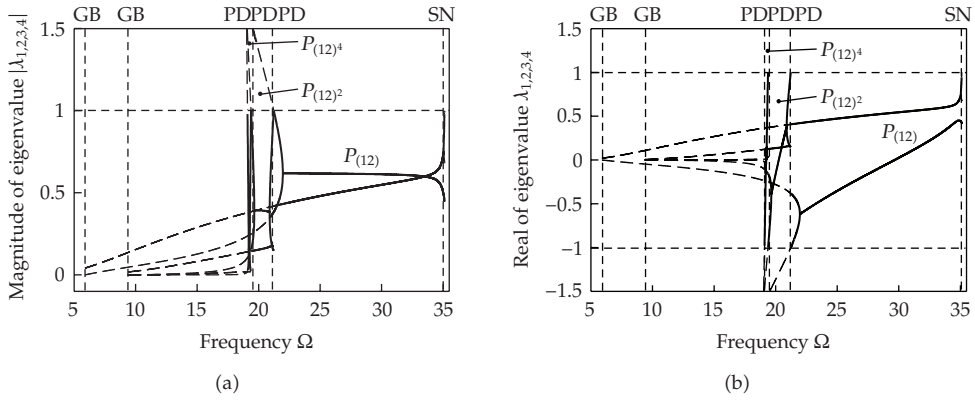

Figure 12: Eigenvalues varying with excitation frequency for $\Omega \in (19.15, 35.20)$: (a) magnitude and (b) real part. Solid and dashed curves represent the stable and unstable solutions, respectively. ($m_1 = 0.01$, $m_2 = 1$, $k = 10$, $c = 6$, $e_1 = 0.9$, $e_2 = 0.7$, $h = 1$, $Q = 0.5$).

the corresponding grazing conditions are given in (3.26) and (3.28). The grazing bifurcations of unstable solutions imply that the corresponding motion relative to a specific mapping structure will disappear in the region of a chaotic motion. The chaotic motion will be switched into another motion with a sudden switching of motion. Both grazing and stick bifurcations give a catastrophe mechanism of the motion switching in the Fermi-acceleration oscillator.

The methodology presented in Section 4 can give the analytical prediction of any periodic motions. For a further demonstration of this technique, consider the same set of parameters except for the range of excitation frequency for the analytical prediction of periodic motions relative to the mapping structures of $P_{(132)^k}$ $(k = 1, 2, 2^2 \cdots)$. With varying excitation frequency, the switching displacements, switching velocities and switching phases of periodic motions of particles, and piston are analytically predicted and presented in Figure 13. The periodic motion of P_{132} is stable for $\Omega \in (3.24, 4.38) \cup (6.57, 7.00)$ and unstable for $\Omega \in (4.38, 6.57)$. The corresponding period-doubling bifurcations occur at $\Omega = 4.38$ and 6.57 and the saddle-node bifurcations occur at $\Omega = 3.24$ and 7.00. The periodic motion of $P_{(132)^2}$ is unstable for $\Omega \in (4.80, 6.31)$ and stable for $\Omega \in (4.38, 4.80) \cup (6.31, 6.57)$. The period-doubling bifurcations of the periodic motion of $P_{(132)^2}$ are at $\Omega = 4.80$ and 6.31, and the corresponding saddle-node bifurcations are at $\Omega = 4.38$ and 6.57. In the vicinity of $\Omega = 4.80$ and 6.31, there are many periodic motions relative to $P_{(132)^4}$, $P_{(132)^8}$, and chaos. Since the ranges of excitation frequency for periodic motions are very small, herein such analytical results will not be presented. For this analytical prediction of periodic motions relative to P_{132} and $P_{(132)^2}$, the corresponding stability and bifurcations of the periodic motions are presented through the magnitudes and real parts of eigenvalues, as shown in Figure 14. For such periodic motions, no grazing and stick bifurcation can be observed. The motion in the range of $\Omega \in (4.80, 6.31)$ is complex periodic motions and chaotic motions.

For a better understanding of the switching dynamics of the Fermi-acceleration oscillator, a parameter map for periodic motions and chaos should be developed from the analytical prediction, and the corresponding local stability and bifurcation conditions with the grazing and stick conditions will be adopted. The parameter map about excitation amplitude and frequency is presented in Figure 15 for parameters ($m_1 = 0.01$, $m_2 = 1$, $k = 10$, $c = 6$, $e_1 = 0.9$, $e_2 = 0.7$, $h = 1$). The "forbidden area" in the parameter map exists because the displacement of piston cannot pass over the location of the fixed wall. In

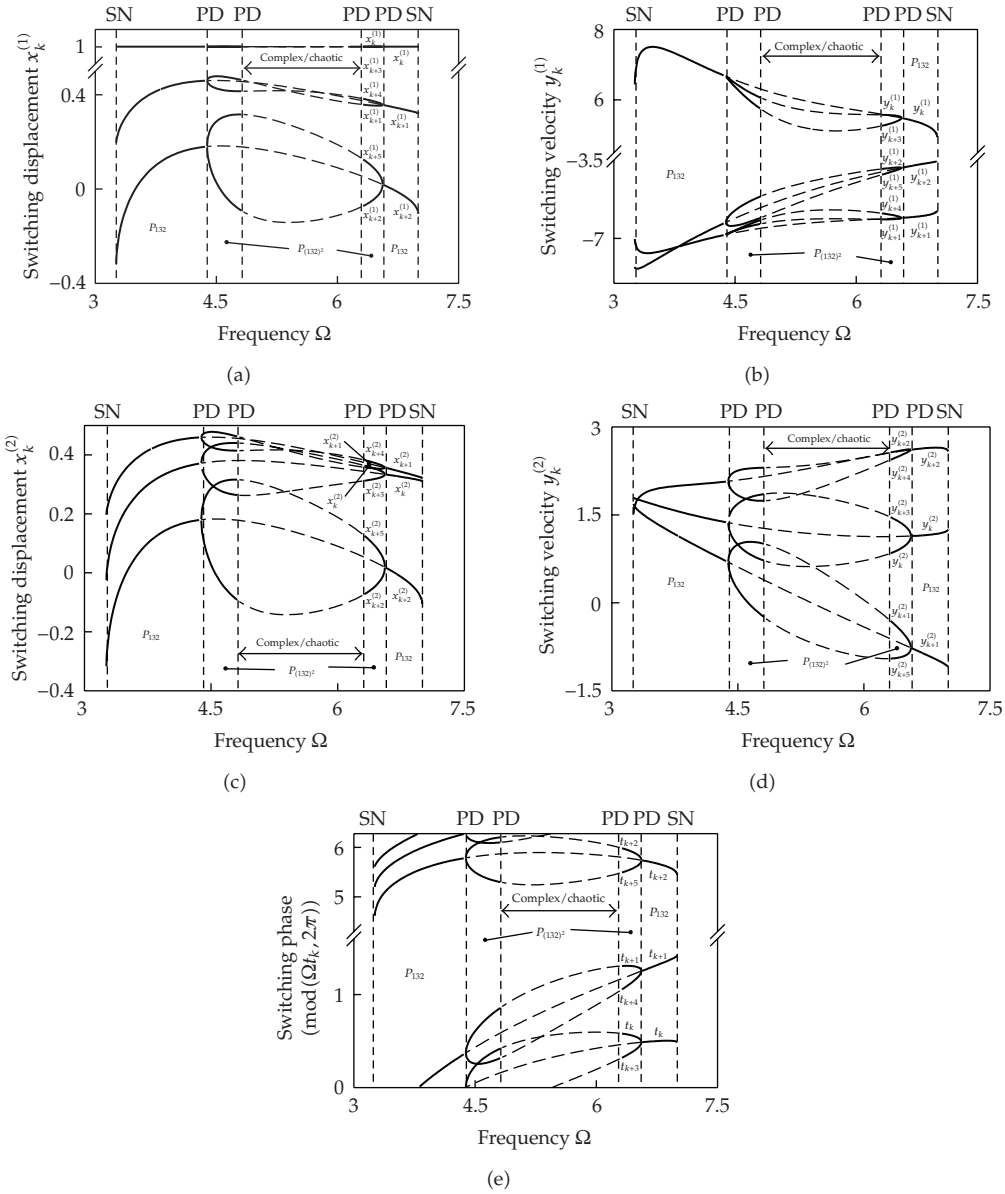

Figure 13: Analytical prediction of periodic motion relative to mapping structure P_{123} for $\Omega \in (3, 7.5)$: (a) switching displacement and (b) switching velocity of the particle; (c) switching displacement and (d) switching velocity of the piston; (e) switching phase. Solid and dashed curves represent the stable and unstable solutions, respectively, ($m_1 = 0.01,\ m_2 = 1,\ k = 10,\ c = 6,\ e_1 = 0.9,\ e_2 = 0.7,\ h = 1,\ Q = 0.5$).

Figure 15(a), the parameter map of (Ω, Q) for $\Omega \in (0, 200)$ and $Q \in (0, 35)$ is presented. Periodic motions of $P_{(12)^k}$ ($k = 1, 2, 2^2, 2^3, \ldots$), $P_{(312)}$, and $P_{(312)^2}$ with complex and chaotic motions are presented. The small regions of periodic motions cannot be clearly illustrated. To illustrate such regions, a zoomed view of the parameter map in such regions is given in Figure 15(b). The regions for periodic motion of $P_{(21)^4}$, P_{312}, and $P_{(312)^2}$ are presented clearly.

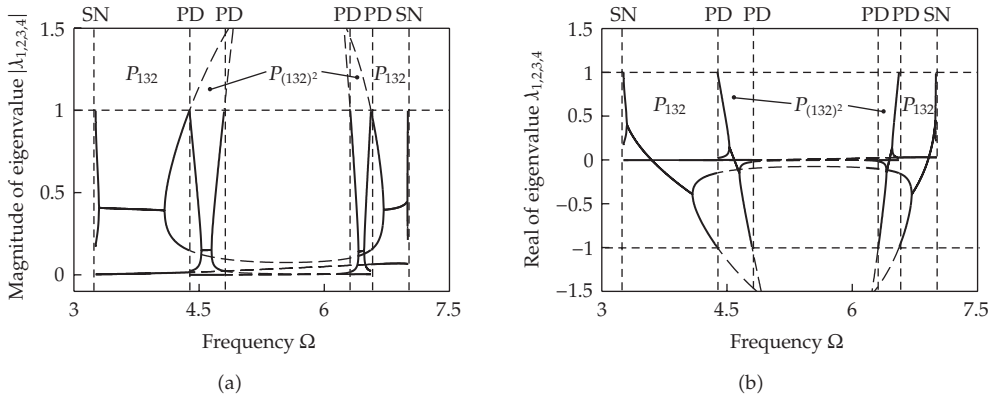

Figure 14: Eigenvalues varying with excitation frequency for $\Omega \in (19.15, 35.20)$: (a) magnitude and (b) real part. Solid and dashed curves represent the stable and unstable solutions, respectively, ($m_1 = 0.01$, $m_2 = 1$, $k = 10$, $c = 6$, $e_1 = 0.9$, $e_2 = 0.7$, $h = 1$, $Q = 0.5$).

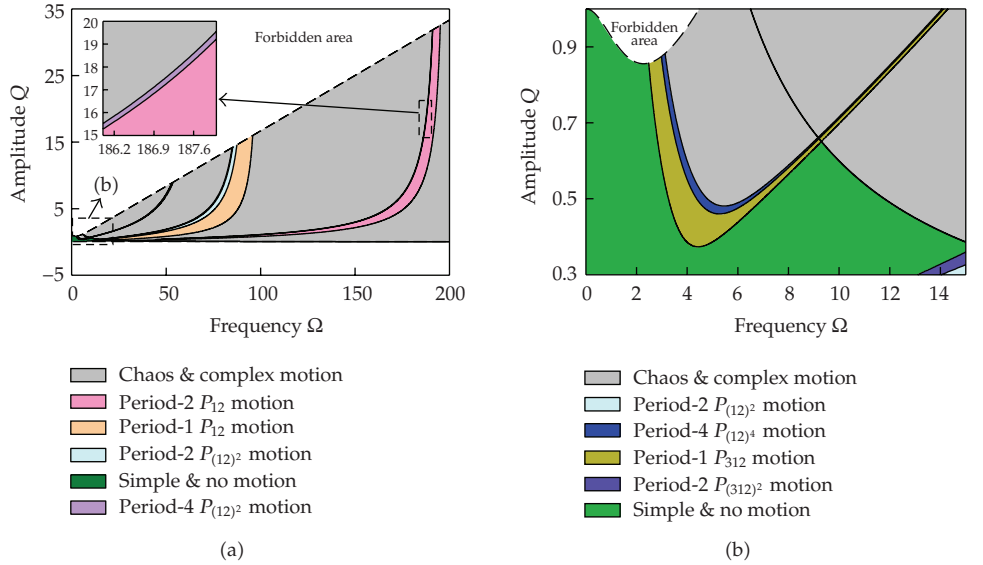

Figure 15: Parameter maps: (a) overall view, (b) zoomed view, ($m_1 = 0.01$, $m_2 = 1$, $k = 10$, $c = 6$, $e_1 = 0.9$, $e_2 = 0.7$, $h = 1$).

5.3. Simulations

From the previous section, periodic motions were analytically predicted. It is significant to illustrate motions for a better understanding of the dynamics of the Fermi-acceleration oscillator. To illustrate motions in the generalized Fermi-acceleration oscillator, the closed-form solutions of particle and piston in the appendix are used again for numerical simulations. As in the section of bifurcation scenario, the corresponding conditions for motion switching should be embedded in the computer program. The time histories of displacement and velocity of both the particle and piston will be presented for periodic motions. In addition, phase planes of both particle and piston will be illustrated. For chaotic motions, the

Poincare mapping sections consisting of the switching points on the switching boundaries will be presented. In numerical illustrations, the switching points are labeled by circular symbols. The large and small circular symbols are for the particle and piston in the Fermi-acceleration oscillator, respectively.

Consider a set of parameters ($m_1 = 0.01,\ m_2 = 1,\ k = 10,\ c = 6,\ e_1 = 0.9,\ e_2 = 0.7,\ h = 1,\ Q = 0.5$) with $\Omega = 6.7$. From the analytical prediction, one obtains the initial condition (i.e., $t_0 = 0.0741633079,\ x_0^{(1)} = 1.0,\ \dot{x}_0^{(1)} = 5.4104888431,\ x_0^{(2)} = 0.3280350633,\ \dot{x}_0^{(2)}$=1.1504459376) for a periodic motion of P_{213}. Using such an initial condition, a numerical simulation gives phase plane and the time histories of displacements and velocities of particle and piston, as shown in Figure 16. The initial conditions are marked by green circular symbols. The arrows give the directions of motions for the particle and piston. The switching points are marked by the hollow circular symbols. The corresponding mappings are labeled by ${}^{(1)}P_\lambda$, ${}^{(2)}P_\lambda$ ($\lambda = 1, 2, 3$). In Figure 16(a), the switching displacements of particle and piston at the impacting points are of the same. However, the switching velocities for both of them are different because impacts cause the velocity to be discontinuous, as shown in Figure 16(b). In Figures 16(a) and 16(b), the solid and dashed curves depict the motions of particle and piston, respectively. When the particle impacts with the fixed wall, the piston motion will not be influenced because the piston moves by itself. Thus, the piston velocity will not be changed. When the impact between the particle and piston occurs, the velocity change of the piston is very small because the particle's mass is much smaller than the piston's mass. If the particle's mass is with the same quantitative level of the piston's mass, the velocity change before and after impacts can be clearly observed. In Figure 16(c), a trajectory of particle for such a periodic motion of P_{213} in phase plane is plotted. The dashed curves are the switching boundary for the particle motion, which is given by the displacement of piston. The periodic motion of particle consists of three pieces of trajectories. Similarly, a trajectory of piston with the corresponding switching boundary for the periodic motion is plotted in Figure 16(d).

As discussed before, there are two kinds of motions for motion switching: (i) stick motion and nonstick motion. In other words, the nonstick motion means that the particle does not stay on the piston, and the stick motion means that the particle stays on the piston and moves together. In Figure 16, the impacting motion of the particle and piston without stick are presented. The stick motion of particle and piston is an important phenomenon. Thus, consider parameters ($m_1 = 0.001,\ m_2 = 1,\ k = 20,\ c = 8,\ e_1 = 0.9,\ e_2 = 0.01,\ h = 1,\ Q = 0.5$) with $\Omega = 6.5$ to demonstrate a periodic motion with stick. From the analytical prediction, one obtains an initial condition ($t_0 = 0.70442282,\ x_0^{(1)} = x_0^{(2)} = -0.38755043,\ \dot{x}_0^{(1)} = \dot{x}_0^{(2)}$=1.97682140) for a periodic motion with stick, which is relative to a mapping structure of P_{03^2}. When such an initial condition is used for a numerical simulation, the corresponding results are presented in Figure 17. Before the stick motion is formed, there are two times of the impact chattering between the particle and piston. In numerical computations, the relative velocity tolerance of the particle and piston at the impact boundary is set to be $|\dot{x}_0^{(1)} - \dot{x}_0^{(2)}| < \varepsilon = 10^{-4}$. Under such a condition, it is assumed that the velocities of particle and piston are of the same. If the chosen impact restriction coefficient is relatively large, this set of parameters is very difficult to observe the periodic motion with stick. The detailed discussion of such impact chattering can be referred to Luo and O'Connor [46, 47]. To observe the stick motion of particle and piston in periodic motions, the acceleration and jerk of particle and piston are very important from the analytical conditions for motion switching in Section 3.3. So the time histories of the displacements, velocities, accelerations and jerks of particle and piston are presented in Figure 17, and the trajectories of particle and piston in phase plane

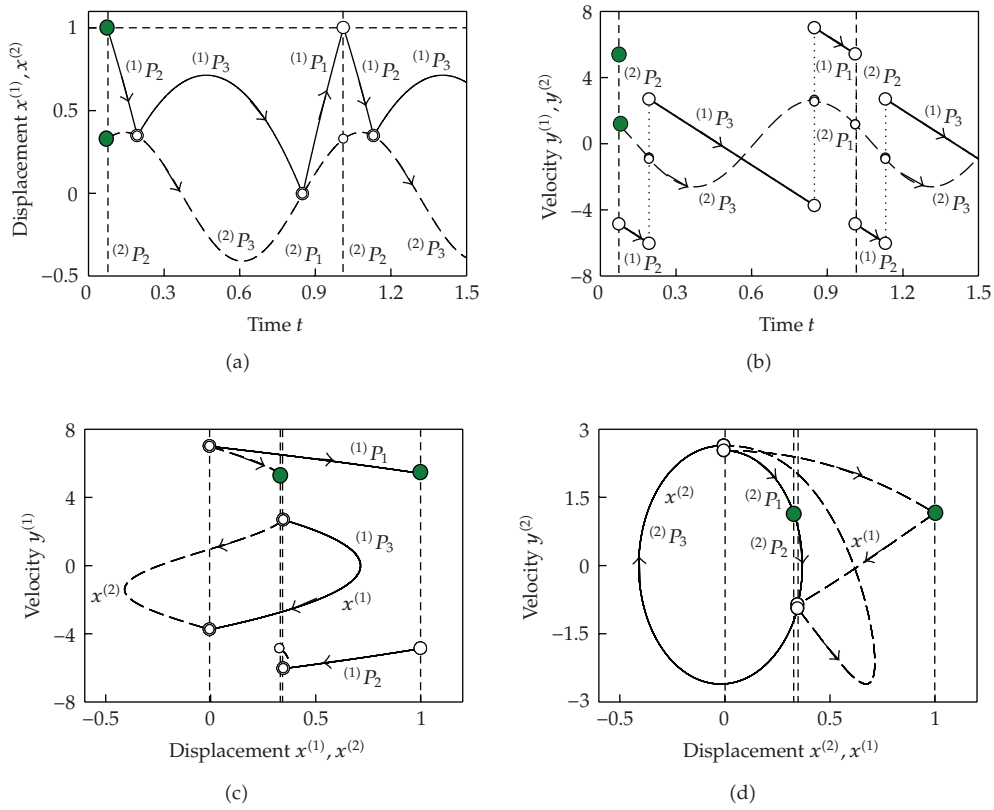

Figure 16: Periodic motion of $P_{(213)}$ ($\Omega = 6.7$ and $e_2 = 0.7$): (a) displacement history, (b) velocity history, (c) phase plane of particle, and (d) phase plane of piston. Solid and dashed curves indicate the motion of particle and piston, respectively, ($m_1 = 0.01$, $m_2 = 1$, $k = 10$, $c = 6$, $e_1 = 0.9$, $h = 1$, $Q = 0.5$, $t_0 = 0.0741633079$, $x_0^{(1)} = 1.0$, $\dot{x}_0^{(1)} = 5.4104888431$, $x_0^{(2)} = 0.3280350633$, $\dot{x}_0^{(2)} = 1.1504459376$).

are plotted in Figure 18. For the nonstick part of motion, the discussion is the same as in Figure 16. For the part of stick motion, the displacement and velocity for particle and piston should be $x^{(1)} = x^{(2)}$ and $\dot{x}^{(1)} = \dot{x}^{(2)}$, as shown in Figures 17(a) and 17(b). Such a stick motion is labeled by $({}^{(1)}P_0, {}^{(2)}P_0)$. The solid and dashed curves depict the motions of particle and piston, respectively. In addition, the condition of stick motion in (3.19) should be satisfied, which is expressed by the relative acceleration (i.e., $g^{(i)} = \ddot{x}^{(i)} - \ddot{x}^{(\bar{i})}$, $i \in \{1, 2\}$) with $a^{(i)} \equiv \ddot{x}^{(i)}$, $a^{(\bar{i})} \equiv \ddot{x}^{(\bar{i})}$. The condition of stick motion (i.e., $g^{(1)} < 0$ or $g^{(2)} > 0$) gives the absolute acceleration relation (i.e., $-g = \ddot{x}^{(1)} < \ddot{x}^{(2)}$) under which the stick motion will be formed. Such a condition of stick motion is observed in the shaded area in Figure 17(c). The vanishing condition of stick motion is given by $g^{(i)} = \ddot{x}^{(i)} - \ddot{x}^{(\bar{i})} = 0$ with the relative jerks $((d/st)g^{(i)} = J^{(i)} - J^{(\bar{i})})$ with $J^{(i)} \equiv \dddot{x}^{(i)}$, $J^{(\bar{i})} \equiv \dddot{x}^{(\bar{i})}$. In other words, $(d/dt)g^{(1)} = J^{(1)} - J^{(2)} > 0$ or $(d/dt)g^{(2)} = J^{(2)} - J^{(1)} < 0$. From such conditions, one obtains $J^{(2)} < J^{(1)} = 0$ from which the stick motion will disappear. Such a condition can be observed in Figures 17(c) and 17(d). For the nonstick motion, the acceleration and jerk for particle are constants (i.e., $a^{(1)} = -g$ and $J^{(1)} = 0$). The dashed curves in Figures 17(c) and 17(d) give the acceleration and jerks for the piston. For a further observation of the analytical condition of stick, the phase plane, acceleration, and

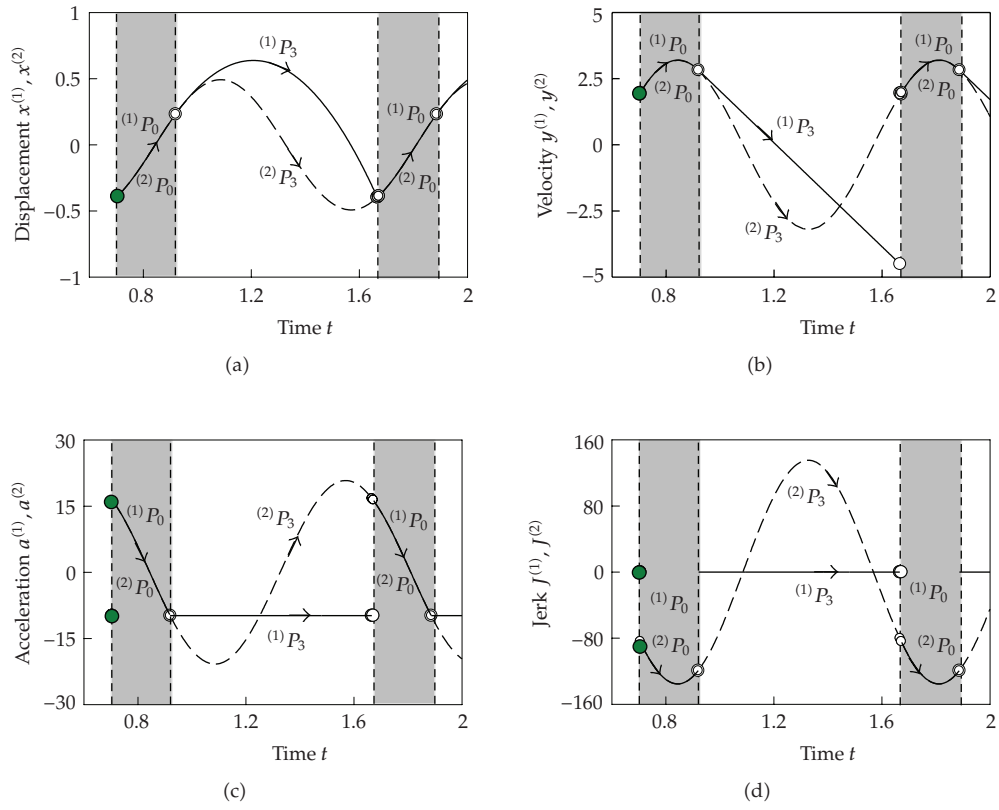

Figure 17: Periodic motion of P_{03^4} ($\Omega = 6.5$ and $e_2 = 0.01$): (a) displacement time-history, (b) velocity time-history, (c) phase plane of particle, and (d) phase plane of piston. Solid and dashed curves represents the motions of particle and piston, respectively, ($m_1 = 0.01,\ m_2 = 1,\ k = 10,\ c = 6,\ e_1 = 0.9,\ h = 1,\ Q = 0.5$) ($t_0 = 0.70442282,\ x_0^{(1)} = -0.38755043,\ \dot{x}_0^{(1)} = 1.90527812,\ x_0^{(2)} = -0.38755043,\ \dot{x}_0^{(2)}$=1.96895970).

jerk versus displacement for particle and piston are presented in Figure 18. In Figures 18(a) and 18(d), the trajectories of periodic motion with stick for particle and piston are presented, and the dashed curves are the displacement boundaries for motion switching. The arrows still show the directions of flows for such a periodic motion. The stick motion portions are shaded by the gray color. It is observed that the displacement and velocity for the stick motion are overlapped. To look into the condition for stick motion, in Figures 18(b), 18(c), 18(e), and 18(f), the vertical arrows show the motion switching at the switching boundaries. At the initial condition (or stick starting point), the acceleration of particle is less than the piston's acceleration (i.e., $a^{(2)} > a^{(1)} = -9.8$) with the same displacement and velocity. So the stick motion will be formed, because the jerk of particle is zero, and the jerk of piston is negative. With increasing time, the acceleration of piston becomes small. Until $a^{(2)} = a^{(1)} = -9.8$, the stick motion should still exist. However, for $a^{(2)} = a^{(1)} = -9.8$, if the jerk of the piston is still negative, then the acceleration of piston will be less than the particle's acceleration. Thus, the stick motion will disappear and the nonstick motion is formed. Such a switching mechanism of the stick motion is clearly observed in Figures 18(b), 18(c), 18(e), and 18(f). Finally, the trajectories in phase plane for a set of periodic motions are presented in Figures 19(a)–19(f) with parameters ($m_1 = 0.001,\ m_2 = 1,\ k = 20,\ c = 8,\ e_1 = 0.9,\ h = 1,\ Q = 0.5$). The mapping

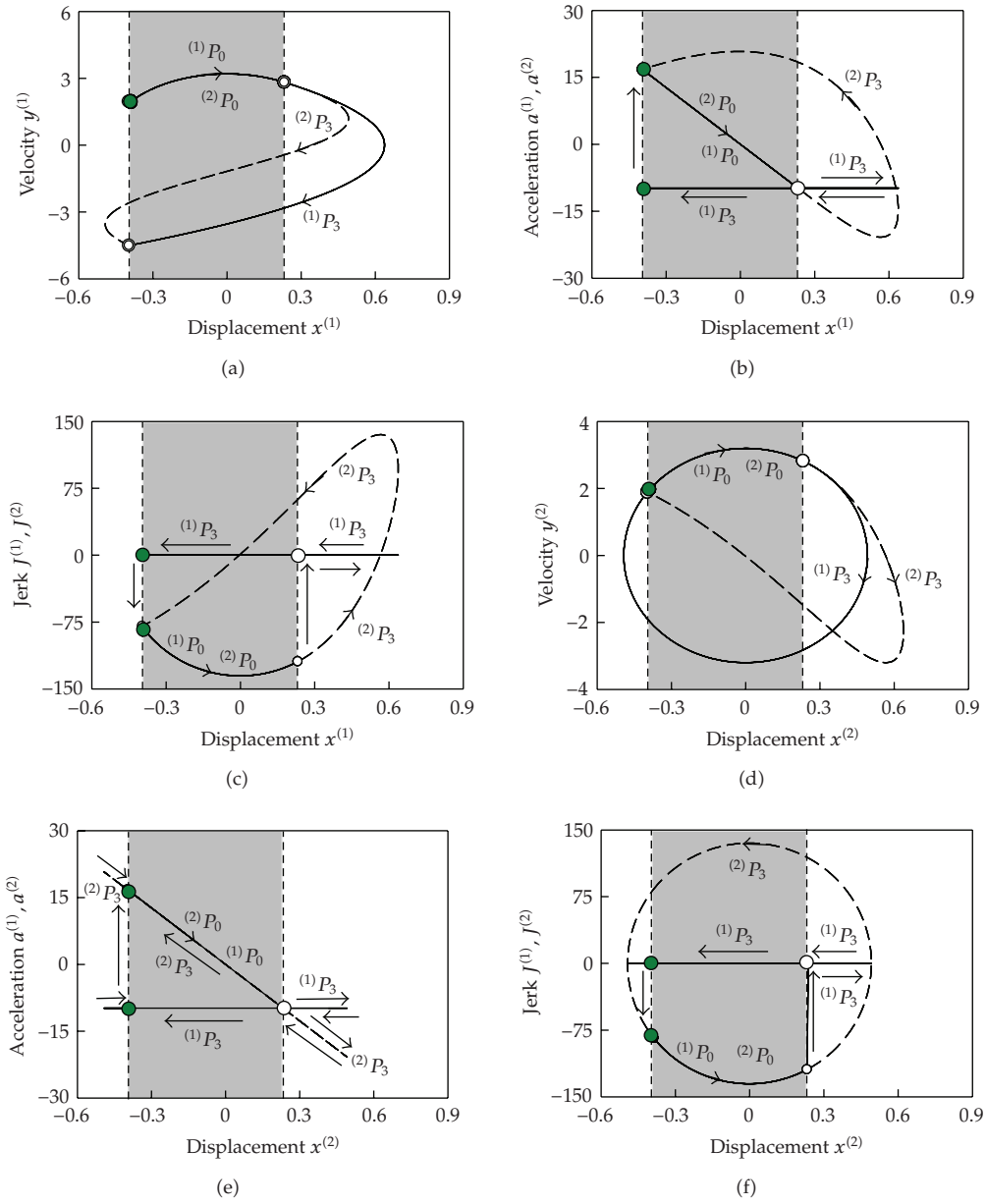

Figure 18: Periodic motion of P_{3^3} ($\Omega = 6.5$ and $e_2 = 0.01$). Particle: (a) phase plane, (b) acceleration and (c) jerks versus displacement of particle. Piston: (d) phase plane, (e) acceleration, and (f) jerks versus displacement of piston, ($m_1 = 0.01$, $m_2 = 1$, $k = 10$, $c = 6$, $e_1 = 0.9$, $h = 1$, $Q = 0.5$) ($t_0 = 0.70442282$, $x_0^{(1)} = -0.38755043$, $\dot{x}_0^{(1)} = 1.90527812$, $x_0^{(2)} = -0.38755043$, $\dot{x}_0^{(2)} = 1.96895970$).

structures, other parameters, and initial conditions are listed in Table 2 for periodic motions. The green points are the starting points (initial points), and the solid and dashed curves represent the motions of particle and piston, respectively. The other periodic motions can be similarly illustrated.

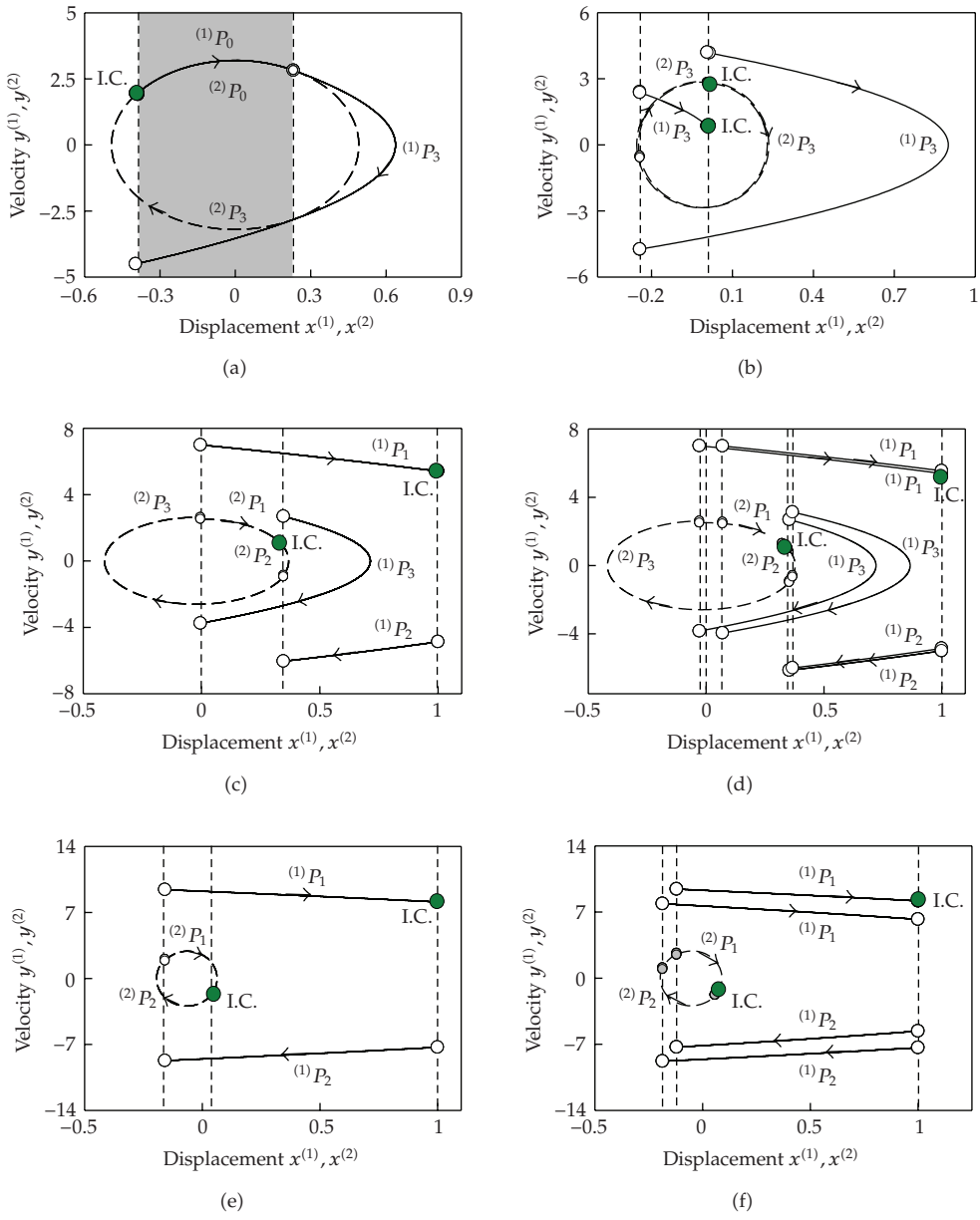

Figure 19: Phase planes. Solid and dashed curves represent motions of particle and piston, respectively, ($m_1 = 0.01$, $m_2 = 1$, $k = 10$, $c = 6$, $e_1 = 0.9$, $Q = 0.5$): (a) P_{03^2} ($\Omega = 6.5$, $e_2 = 0.01$) ($t_0 = 0.70442282$, $x_0^{(1)} = x_0^{(2)} = -0.38755043$, $\dot{x}_0^{(1)} = 1.90527812$, $\dot{x}_0^{(2)} = 1.96895970$), (b) P_{3^2} ($\Omega = 11.8$, $e_2 = 0.01$) ($t_0 = 0.51035890$, $x_0^{(1)} = x_0^{(2)} = 0.01422235$, $\dot{x}_0^{(1)} = 0.87719897$, $\dot{x}_0^{(2)} = 2.83304464$), (c) $P_{(213)}$ ($\Omega = 6.7$, $e_2 = 0.7$) ($t_0 = 0.07416331$, $x_0^{(1)} = 1.0$, $\dot{x}_0^{(1)} = 5.41048884$, $x_0^{(2)} = 0.32803506$, $\dot{x}_0^{(2)} = 1.15044594$), (d) $P_{(213)^2}$ ($\Omega = 6.5$, $e_2 = 0.7$) ($t_0 = 0.08347153$, $x_0^{(1)} = 1.0$, $\dot{x}_0^{(1)} = 5.54878710$, $x_0^{(2)} = 0.34730036$, $\dot{x}_0^{(2)} = 0.98801503$), (e) P_{12} ($\Omega = 22.7$, $e_2 = 0.7$) ($t_0 = 0.08699328$, $x_0^{(1)} = 1.0$, $\dot{x}_0^{(1)} = 8.11298196$, $x_0^{(2)} = 0.04059727$, $\dot{x}_0^{(2)} = -1.64929089$), and (f) $P_{(12)^2}$ ($\Omega = 20.4$, $e_2 = 0.7$) ($t_0 = 0.39975776$, $x_0^{(1)} = 1.0$, $\dot{x}_0^{(1)} = 8.17571963$, $x_0^{(2)} = 0.07102098$, $\dot{x}_0^{(2)} = -1.44790328$).

Table 2: Initial conditions for periodic motions ($m_1 = 0.01$, $m_2 = 1$, $k = 10$, $c = 6$, $e_1 = 0.9$, $h = 1$, $Q = 0.5$).

Mapping	(Ω, e_2)	Initial time t_0	$(x_0^{(1)}, \dot{x}_0^{(1)})$	$(x_0^{(2)}, \dot{x}_0^{(2)})$
P_{3^20}	(6.5, 0.01)	0.70490614	(−0.38755043, 1.97682140)	(−0.38755043, 1.97682140)
P_{3^2}	(11.8, 0.01)	0.51035890	(0.01422235, 0.87719897)	(0.01422235, 2.83304464)
$P_{(213)}$	(6.7, 0.7)	0.07416331	(1.0, 5.41048884)	(0.32803506, 1.15044594)
$P_{(213)^2}$	(6.5, 0.7)	0.08347153	(1.0, 5.54878710)	(0.34730036, 0.98801503)
P_{12}	(22.7, 0.7)	0.08699328	(1.0, 8.11298196)	(0.04059727, −1.64929089)
$P_{(12)^2}$	(20.4, 0.7)	0.39975776	(1.0, 8.17571963)	(0.07102098, −1.44790328)

Finally, a chaotic motion relative to $P_{\ldots 21212121333}$ is illustrated for parameters ($m_1 = 0.01$, $m_2 = 1$, $k = 10$, $c = 6$, $e_1 = 0.9$, $e_2 = 0.7$, $h = 1$, $Q = 0.5$, $\Omega = 12$) and the initial conditions ($t_0 = 0.40024561$, $x_0^{(1)} = x_0^{(2)} = -0.22472018$, $\dot{x}_0^{(1)} = 2.58913681$, $\dot{x}_0^{(2)}$=1.19198278) are used. The time histories of displacement and velocity of particles and piston are presented in Figures 20(a) and 20(b), respectively. In addition, the trajectories of particle and piston in phase plane are plotted in Figures 20(c) and 20(d), accordingly. The particle motion is very chaotic and such a chaotic motion of particle takes a big region in phase plane. However, the trajectory of piston is in a small region of ring in phase plane. This is because the particle's mass is much smaller than the piston's mass. The impact effect on the particle motion is much bigger than on the piston motion. To further looking into the chaotic behavior of this motion, the corresponding Poincare mapping sections for such chaotic motion are presented in Figure 21. The Poincare mapping sections consist of the switching points on the switching boundaries. In Figure 21(a) and **??**, the switching displacement ($x_k^{(1)}$) and velocity ($\dot{x}_k^{(1)}$) versus switching phase ($\mathrm{mod}\,(\Omega t_k, 2\pi)$) for the particle are presented. The switching displacement and velocity of piston versus switching phase ($\mathrm{mod}\,(\Omega t_k, 2\pi)$) are also illustrated in Figures 21(c) and 21(d), respectively. The Poincare mapping sections in phase space for the particle and piston are shown in Figures 21(e) and 21(f), respectively. Again, because the particle's mass is chosen to be much smaller than the piston's mass, the impact effect on the piston is not very obvious. Therefore, one often assumed the piston have a fixed sinusoidal motion. Once the particle's mass is not much less than the piston's mass, the impact effect on the piston motion will become significant. The aforementioned assumption should not be adequate. For a further investigation of chaos in such a Fermi-acceleration oscillator, the Lyapunov exponent can be used, and the scaling properties of chaotic motions can be studied. This paper mainly focuses on the motion switching of the multimotion states. Therefore, the other investigations on nonlinear dynamics of the generalized Fermi-acceleration oscillator can be performed in sequel.

6. Conclusion

In this paper, the mechanism of motion switching of a particle in such a generalized Fermi-oscillator was studied through the theory of discontinuous dynamical systems, and the corresponding analytical conditions for the motion switching were developed. From the solutions of linear systems in each domain, the generic mappings are introduced. Further, the

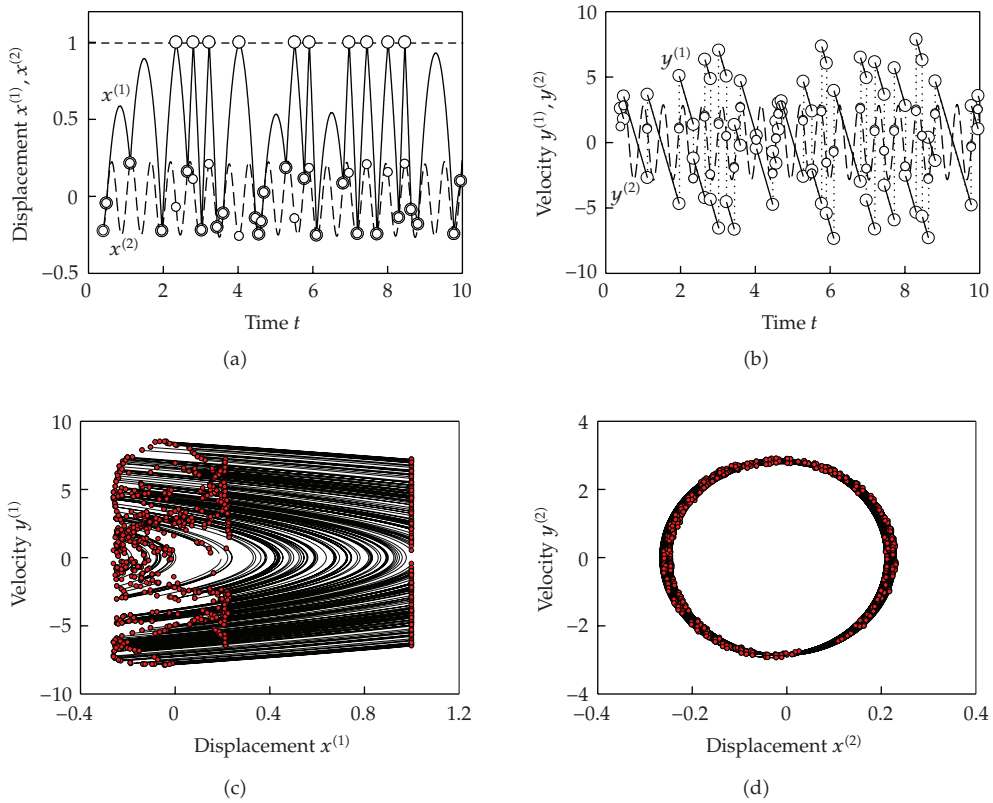

Figure 20: Chaotic motion ($\Omega = 12$): (a) displacement time-history, (b) velocity time-history, (c) phase plane for particle, and (d) phase plane for piston. Solid and dashed curves represent the motion of particle and piston, respectively, ($m_1 = 0.01$, $m_2 = 1$, $k = 10$, $c = 6$, $e_1 = 0.9$, $e_2 = 0.7$, $h = 1$, $Q = 0.5$) and the initial condition ($t_0 = 0.40024561$, $x_0^{(1)} = x_0^{(2)} = -0.22472018$, $\dot{x}_0^{(1)} = 2.58913681$, $\dot{x}_0^{(2)} = 1.19198278$).

mapping structures for periodic motions were developed, and such periodic motions in the Fermi-acceleration oscillator were predicted analytically. The corresponding local stability and bifurcation are carried out. From the analytical prediction, parameter maps of regular and chaotic motions were achieved for a global view of motions in the Fermi-acceleration oscillator. Illustrations of periodic and chaotic motions in such an oscillator were done. This methodology will provide a useful way to determine dynamical behaviors in the Fermi-acceleration oscillator.

Appendix

Equation of motion for the particle in the generalized Fermi-oscillator is

$$\ddot{x}^{(1)} = -g. \tag{A.1}$$

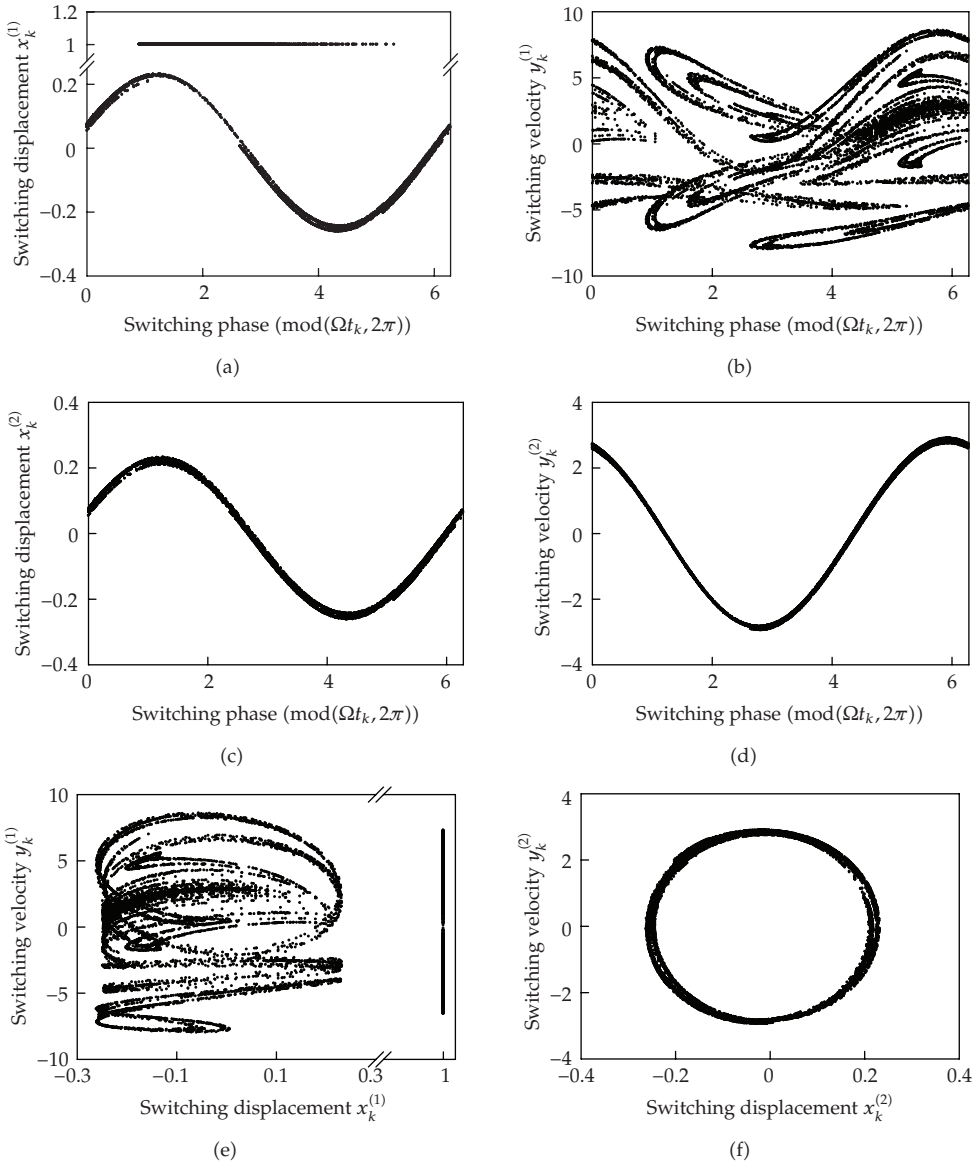

Figure 21: Poincare mapping sections of chaotic motion ($\Omega = 12$). (a) Switching displacement of particle, (b) switching velocity of particle, (c) switching displacement of piston, (d) switching velocity of piston, (e) Poincare section of particle, and (f) Poincare section of piston. ($m_1 = 0.01$, $m_2 = 1$, $k = 10$, $c = 6$, $e_1 = 0.9$, $e_2 = 0.7$, $h = 1$, $Q = 0.5$) and initial condition ($t_0 = 0.40024561$, $x_0^{(1)} = x_0^{(2)} = -0.22472018$, $\dot{x}_0^{(1)} = 2.58913681$, $\dot{x}_0^{(2)} = 1.19198278$).

The solution for the particle motion is

$$\dot{x}^{(1)} = \dot{x}_k^{(1)} - g\left(t - t_k\right),$$
$$x^{(1)} = x_k^{(1)} + \dot{x}_k^{(1)}\left(t - t_k\right) - \frac{1}{2}g\left(t - t_k\right)^2. \tag{A.2}$$

Solution for Piston

The equation of motion for piston and stick motion in the extended Fermi-oscillator is

$$\ddot{x}^{(\alpha)} + 2d^{(\alpha)}\dot{x}^{(\alpha)} + \left(\omega^{(\alpha)}\right)^2 x^{(\alpha)} = \left(\omega^{(\alpha)}\right)^2 Q\cos\Omega t - 2d^{(\alpha)}Q\Omega\sin\Omega t. \tag{A.3}$$

Superscript indices ($\alpha = 0, 2$) denote stick and nonstick motions of piston, respectively. The subscripts k and $k+1$ represent the initial and final states.

Case 1 ($d^{(\alpha)} = \omega^{(\alpha)}$).

$$\begin{aligned}
x^{(\alpha)} &= \left[C_1^{(\alpha)} + C_2^{(\alpha)}(t - t_k)\right]e^{r_1^{(\alpha)}(t-t_k)} + A^{(\alpha)}\cos\Omega t + B^{(\alpha)}\sin\Omega t,\\
\dot{x}^{(\alpha)} &= C_2^{(\alpha)}e^{r_1^{(\alpha)}(t-t_k)} + r_1^{(\alpha)}\left[C_1^{(\alpha)} + C_2^{(\alpha)}(t - t_k)\right]e^{r_1^{(\alpha)}(t-t_k)}\\
&\quad - A^{(\alpha)}\Omega\sin\Omega t + B^{(\alpha)}\Omega\cos\Omega t,\\
\ddot{x}^{(\alpha)} &= 2r_1^{(\alpha)}C_2^{(\alpha)}e^{r_1^{(\alpha)}(t-t_k)} + \left(r_1^{(\alpha)}\right)^2\left[C_1^{(\alpha)} + C_2^{(\alpha)}(t - t_k)\right]e^{r_1^{(\alpha)}(t-t_k)}\\
&\quad - A^{(\alpha)}\Omega^2\cos\Omega t - B^{(\alpha)}\Omega^2\sin\Omega t,
\end{aligned} \tag{A.4}$$

where

$$\begin{aligned}
C_1^{(\alpha)} &= x_k^{(\alpha)} - A^{(\alpha)}\cos\Omega t_k - B^{(\alpha)}\sin\Omega t_k,\\
C_2^{(\alpha)} &= \dot{x}_k^{(\alpha)} + A^{(\alpha)}\Omega\sin\Omega t_k - B^{(\alpha)}\Omega\cos\Omega t_k - r_1^{(\alpha)}C_1^{(\alpha)},\\
A^{(\alpha)} &= \frac{\left(\omega^{(\alpha)}\right)^2 Q\left[\left(\omega^{(\alpha)}\right)^2 - \Omega^2\right] + 4\left(d^{(\alpha)}\right)^2\Omega^2 Q}{4\left(d^{(\alpha)}\right)^2\Omega^2 + \left[\left(\omega^{(\alpha)}\right)^2 - \Omega^2\right]^2},\\
B^{(\alpha)} &= \frac{2d^{(\alpha)}\Omega^3 Q}{4\left(d^{(\alpha)}\right)^2\Omega^2 + \left[\left(\omega^{(\alpha)}\right)^2 - \Omega^2\right]^2},\\
r_1^{(\alpha)} &= -d^{(\alpha)}.
\end{aligned} \tag{A.5}$$

Case 2 ($d^{(\alpha)} > \omega^{(\alpha)}$).

$$\begin{aligned}
x^{(\alpha)} &= C_1^{(\alpha)}e^{r_1^{(\alpha)}(t-t_k)} + C_2^{(\alpha)}e^{r_2^{(\alpha)}(t-t_k)} + A^{(\alpha)}\cos\Omega t + B^{(\alpha)}\sin\Omega t,\\
\dot{x}^{(\alpha)} &= C_1^{(\alpha)}r_1^{(\alpha)}e^{r_1^{(\alpha)}(t-t_k)} + C_2^{(\alpha)}r_2^{(\alpha)}e^{r_2^{(\alpha)}(t-t_k)} - A^{(\alpha)}\Omega\sin\Omega t + B^{(\alpha)}\Omega\cos\Omega t,\\
\ddot{x}^{(\alpha)} &= C_1^{(\alpha)}\left(r_1^{(\alpha)}\right)^2 e^{r_1^{(\alpha)}(t-t_k)} + C_2^{(\alpha)}\left(r_2^{(\alpha)}\right)^2 e^{r_2^{(\alpha)}(t-t_k)} - A^{(\alpha)}\Omega^2\cos\Omega t - B^{(\alpha)}\Omega^2\sin\Omega t,
\end{aligned} \tag{A.6}$$

where

$$
\begin{aligned}
C_1^{(\alpha)} &= \frac{r_2^{(\alpha)}\left(x_k^{(\alpha)} - A^{(\alpha)}\cos\Omega t_k - B^{(\alpha)}\sin\Omega t_k\right) - A^{(\alpha)}\Omega\sin\Omega t_k + B^{(\alpha)}\Omega\cos\Omega t_k - \dot{x}_k^{(\alpha)}}{r_2^{(\alpha)} - r_1^{(\alpha)}},\\
C_2^{(\alpha)} &= x_k^{(\alpha)} - A^{(\alpha)}\cos\Omega t_k - B^{(\alpha)}\sin\Omega t_k - C_1^{(\alpha)},\\
A^{(\alpha)} &= \frac{\left(\omega^{(\alpha)}\right)^2 Q\left[\left(\omega^{(\alpha)}\right)^2 - \Omega^2\right] + 4\left(d^{(\alpha)}\right)^2\Omega^2 Q}{4\left(d^{(\alpha)}\right)^2\Omega^2 + \left[\left(\omega^{(\alpha)}\right)^2 - \Omega^2\right]^2},\\
B^{(\alpha)} &= \frac{2d^{(\alpha)}\Omega^3 Q}{4\left(d^{(\alpha)}\right)^2\Omega^2 + \left[\left(\omega^{(\alpha)}\right)^2 - \Omega^2\right]^2},\\
r_{1,2}^{(\alpha)} &= -d^{(\alpha)} \pm \sqrt{\left(d^{(\alpha)}\right)^2 - \left(\omega^{(\alpha)}\right)^2}.
\end{aligned}
\tag{A.7}
$$

Case 3 ($d^{(\alpha)} < \omega^{(\alpha)}$).

$$
\begin{aligned}
x^{(\alpha)} &= e^{-d^{(\alpha)}(t-t_k)}\left[C_1^{(\alpha)}\cos\omega_d^{(\alpha)}(t-t_k) + C_2^{(\alpha)}\sin\omega_d^{(\alpha)}(t-t_k)\right] + A^{(\alpha)}\cos\Omega t + B^{(\alpha)}\sin\Omega t,\\
\dot{x}^{(\alpha)} &= e^{-d^{(\alpha)}(t-t_k)}\left(-d^{(\alpha)}C_2^{(\alpha)} - C_1^{(\alpha)}\omega_d^{(\alpha)}\right)\sin\omega_d^{(\alpha)}(t-t_k)\\
&\quad + e^{-d^{(\alpha)}(t-t_k)}\left(-d^{(\alpha)}C_1^{(\alpha)} + C_2^{(\alpha)}\omega_d^{(\alpha)}\right)\cos\omega_d^{(\alpha)}(t-t_k)\\
&\quad - A^{(\alpha)}\Omega\sin\Omega t + B^{(\alpha)}\Omega\cos\Omega t,\\
\ddot{x}^{(\alpha)} &= e^{-d^{(\alpha)}(t-t_k)}\left\{\left[\left(d^{(\alpha)}\right)^2 - \left(\omega_d^{(\alpha)}\right)^2\right]C_2^{(\alpha)} + 2d^{(\alpha)}\omega_d^{(\alpha)}C_1^{(\alpha)}\right\}\sin\omega_d^{(\alpha)}(t-t_k)\\
&\quad + e^{-d^{(\alpha)}(t-t_k)}\left\{\left[\left(d^{(\alpha)}\right)^2 - \left(\omega_d^{(\alpha)}\right)^2\right]C_1^{(\alpha)} - 2d^{(\alpha)}\omega_d^{(\alpha)}C_2^{(\alpha)}\right\}\cos\omega_d^{(\alpha)}(t-t_k)\\
&\quad - A^{(\alpha)}\Omega^2\cos\Omega t - B^{(\alpha)}\Omega^2\sin\Omega t,
\end{aligned}
\tag{A.8}
$$

where

$$
\begin{aligned}
C_1^{(\alpha)} &= x_k^{(\alpha)} - A^{(\alpha)}\cos\Omega t_k - B^{(\alpha)}\sin\Omega t_k,\\
C_2^{(\alpha)} &= \frac{\dot{x}_k^{(\alpha)} + A^{(\alpha)}\Omega\sin\Omega t_k - B^{(\alpha)}\Omega\cos\Omega t_k + d^{(\alpha)}C_1^{(\alpha)}}{\omega_d^{(\alpha)}},\\
A^{(\alpha)} &= \frac{\left(\omega^{(\alpha)}\right)^2 Q\left[\left(\omega^{(\alpha)}\right)^2 - \Omega^2\right] + 4\left(d^{(\alpha)}\right)^2\Omega^2 Q}{4\left(d^{(\alpha)}\right)^2\Omega^2 + \left[\left(\omega^{(\alpha)}\right)^2 - \Omega^2\right]^2},\\
B^{(\alpha)} &= \frac{2d^{(\alpha)}\Omega^3 Q}{4\left(d^{(\alpha)}\right)^2\Omega^2 + \left[\left(\omega^{(\alpha)}\right)^2 - \Omega^2\right]^2},\\
\omega_d^{(\alpha)} &= \sqrt{\left(\omega^{(\alpha)}\right)^2 - \left(d^{(\alpha)}\right)^2}.
\end{aligned}
\tag{A.9}
$$

References

[1] E. Fermi, "On the origin of the cosmic radiation," *Physical Review*, vol. 75, no. 8, pp. 1169–1174, 1949.

[2] S. M. Ulam, "On some statistical properties of dynamical systems," in *Proceedings of the 4th Berkeley Symposium on Mathematical Statistics and Probability*, vol. 3, pp. 315–320, University of California Press, Berkeley, Calif, USA, June-July 1961.

[3] G. M. Zaslavskii and B. V. Chirikov, "Fermi acceleration mechanism in the one-dimensional case," *Doklady Akademii Nauk SSSR*, vol. 159, pp. 306–309, 1964.

[4] M. A. Lieberman and A. J. Lichtenberg, "Stochastic and adiabatic behavior of particles accelerated by periodic forces," *Physical Review A*, vol. 5, no. 4, pp. 1852–1866, 1972.

[5] A. J. Lichtenberg and M. A. Lieberman, *Regular and Chaotic Dynamics*, vol. 38 of *Applied Mathematical Sciences*, Springer, New York, NY, USA, 2nd edition, 1992.

[6] L. D. Pustyl'nikov, "Stable and oscillating motions in non-autonomous dynamical systems," *Transactions of the Moscow Mathematical Society*, vol. 14, pp. 1–101, 1978.

[7] L. D. Pustyl'nikov, "Poincaré models, rigorous justification of the second law of thermodynamics from mechanics, and the Fermi acceleration mechanism," *Russian Mathematical Surveys*, vol. 50, no. 1, pp. 145–189, 1995.

[8] J. V. Jose and R. Cordery, "Study of a quantum Fermi-acceleration model," *Physical Review Letters*, vol. 56, no. 4, pp. 290–293, 1986.

[9] S. Celaschi and R. L. Zimmerman, "Evolution of a two-parameter chaotic dynamics from universal attractors," *Physics Letters A*, vol. 120, no. 9, pp. 447–451, 1987.

[10] Z. J. Kowalik, M. Franaszek, and P. Pierański, "Self-reanimating chaos in the bouncing-ball system," *Physical Review A. Third Series*, vol. 37, no. 10, pp. 4016–4022, 1988.

[11] G. A. Luna-Acosta, "Regular and chaotic dynamics of the damped Fermi accelerator," *Physical Review A*, vol. 42, no. 12, pp. 7155–7162, 1990.

[12] S. Warr, W. Cooke, R. C. Ball, and J. M. Huntley, "Probability distribution functions for a single-particle vibrating in one dimension: experimental study and theoretical analysis," *Physica A*, vol. 231, no. 4, pp. 551–574, 1996.

[13] F. Saif, I. Bialynicki-Birula, M. Fortunato, and W. P. Schleich, "Fermi accelerator in atom optics," *Physical Review A*, vol. 58, no. 6, pp. 4779–4783, 1998.

[14] V. Lopac and V. Dananić, "Energy conservation and chaos in the gravitationally driven Fermi oscillator," *American Journal of Physics*, vol. 66, no. 10, pp. 892–902, 1998.

[15] F. Bouchet, F. Cecconi, and A. Vulpiani, "Minimal stochastic model for Fermi's acceleration," *Physical Review Letters*, vol. 92, no. 4, Article ID 040601, 4 pages, 2004.

[16] E. D. Leonel, P. V. E. McClintock, and J. K. L. da Silva, "Fermi-Ulam accelerator model under scaling analysis," *Physical Review Letters*, vol. 93, no. 1, Article ID 014101, 4 pages, 2004.

[17] E. D. Leonel, J. K. L. da Silva, and S. O. Kamphorst, "On the dynamical properties of a Fermi accelerator model," *Physica A*, vol. 331, no. 3-4, pp. 435–447, 2004.

[18] E. D. Leonel and P. V. E. McClintock, "Dissipative area-preserving one-dimensional Fermi accelerator model," *Physical Review E*, vol. 73, no. 6, Article ID 066223, 5 pages, 2006.

[19] E. D. Leonel and R. E. de Carvalho, "A family of crisis in a dissipative Fermi accelerator model," *Physics Letters A*, vol. 364, no. 6, pp. 475–479, 2007.

[20] A. K. Karlis, P. K. Papachristou, F. K. Diakonos, V. Constantoudis, and P. Schmelcher, "Fermi acceleration in the randomized driven Lorentz gas and the Fermi-Ulam model," *Physical Review E*, vol. 76, no. 1, Article ID 016214, 17 pages, 2007.

[21] E. D. Leonel and M. R. Silva, "A bouncing ball model with two nonlinearities: a prototype for Fermi acceleration," *Journal of Physics A*, vol. 41, no. 1, Article ID 015104, 13 pages, 2008.

[22] S. O. Kamphorst, E. D. Leonel, and J. K. L. da Silva, "The presence and lack of Fermi acceleration in nonintegrable billiards," *Journal of Physics A*, vol. 40, no. 37, pp. F887–F893, 2007.

[23] E. D. Leonel and A. L. P. Livorati, "Describing Fermi acceleration with a scaling approach: the Bouncer model revisited," *Physica A*, vol. 387, no. 5-6, pp. 1155–1160, 2008.

[24] D. G. Ladeira and J. K. L. da Silva, "Scaling features of a breathing circular billiard," *Journal of Physics A*, vol. 41, no. 36, Article ID 365101, 13 pages, 2008.

[25] P. J. Holmes, "The dynamics of repeated impacts with a sinusoidally vibrating table," *Journal of Sound and Vibration*, vol. 84, no. 2, pp. 173–189, 1982.

[26] C. N. Bapat, N. Popplewell, and K. McLachlan, "Stable periodic motions of an impact-pair," *Journal of Sound and Vibration*, vol. 87, no. 1, pp. 19–40, 1983.

[27] S. W. Shaw and P. J. Holmes, "A periodically forced piecewise linear oscillator," *Journal of Sound and Vibration*, vol. 90, no. 1, pp. 129–155, 1983.
[28] G. S. Whiston, "Global dynamics of a vibro-impacting linear oscillator," *Journal of Sound and Vibration*, vol. 118, no. 3, pp. 395–424, 1987.
[29] C. N. Bapat and C. Bapat, "Impact-pair under periodic excitation," *Journal of Sound and Vibration*, vol. 120, no. 1, pp. 53–61, 1988.
[30] A. B. Nordmark, "Non-periodic motion caused by grazing incidence in an impact oscillator," *Journal of Sound and Vibration*, vol. 145, no. 2, pp. 279–297, 1991.
[31] S. Foale and S. R. Bishop, "Dynamical complexities of forced impacting systems," *Philosophical Transactions of the Royal Society of London. Series A*, vol. 338, no. 1651, pp. 547–556, 1992.
[32] C. Budd and F. Dux, "Chattering and related behavior in impact oscillators," *Philosophical Transactions: Physical Sciences and Engineering*, vol. 347, pp. 365–389, 1994.
[33] S. Foale, "Analytical determination of bifurcations in an impact oscillator," *Philosophical Transactions: Physical Sciences and Engineering*, vol. 347, no. 1683, pp. 353–364, 1994.
[34] C. N. Bapat, "The general motion of an inclined impact damper with friction," *Journal of Sound and Vibration*, vol. 184, no. 3, pp. 417–427, 1995.
[35] A. C. J. Luo and R. P. S. Han, "The dynamics of a bouncing ball with a sinusoidally vibrating table revisited," *Nonlinear Dynamics*, vol. 10, no. 1, pp. 1–18, 1996.
[36] A. C. J. Luo, "An unsymmetrical motion in a horizontal impact oscillator," *Journal of Vibration and Acoustics*, vol. 124, no. 3, pp. 420–426, 2002.
[37] S. Giusepponi, F. Marchesoni, and M. Borromeo, "Randomness in the bouncing ball dynamics," *Physica A*, vol. 351, no. 1, pp. 142–158, 2005.
[38] A. C. J. Luo, "Period-doubling induced chaotic motion in the LR model of a horizontal impact oscillator," *Chaos, Solitons & Fractals*, vol. 19, no. 4, pp. 823–839, 2004.
[39] A. C. J. Luo, "The mapping dynamics of periodic motions for a three-piecewise linear system under a periodic excitation," *Journal of Sound and Vibration*, vol. 283, no. 3–5, pp. 723–748, 2005.
[40] A. C. J. Luo, "A theory for non-smooth dynamic systems on the connectable domains," *Communications in Nonlinear Science and Numerical Simulation*, vol. 10, no. 1, pp. 1–55, 2005.
[41] A. C. J. Luo, *Singularity and Dynamics on Discontinuous Vector Fields*, vol. 3 of *Monograph Series on Nonlinear Science and Complexity*, Elsevier, Amsterdam, The Netherlands, 2006.
[42] A. C. J. Luo and L. Chen, "Grazing phenomena and fragmented strange attractors in a harmonically forced, piecewise, linear system with impacts," *Proceedings of the Institution of Mechanical Engineers, Part K*, vol. 220, no. 1, pp. 35–51, 2006.
[43] A. C. J. Luo and B. C. Gegg, "Stick and non-stick periodic motions in periodically forced oscillators with dry friction," *Journal of Sound and Vibration*, vol. 291, no. 1-2, pp. 132–168, 2006.
[44] A. C. J. Luo, "On flow switching bifurcations in discontinuous dynamical systems," *Communications in Nonlinear Science and Numerical Simulation*, vol. 12, no. 1, pp. 100–116, 2007.
[45] A. C. J. Luo and B. M. Rapp, "Switching dynamics of a periodically forced discontinuous system with an inclined boundary," in *Proceedings of the ASME International Design Engineering Technical Conferences & Computers and Information in Engineering Conference (DETC '07)*, vol. 5, pp. 239–250, Las Vegas, Nev, USA, September 2008.
[46] A. C. J. Luo and D. O'Connor, "Mechanism of impacting chatter with stick in gear transmission systems," *International Journal of bifurcation and Chaos*. In press.
[47] A. C. J. Luo and D. O'Connor, "Periodic motions and chaos with impacting chatter and stick in gear transmission systems," *International Journal of Bifurcation and Chaos*. In press.
[48] A. C. J. Luo, "On the differential geometry of flows in nonlinear dynamical systems," *Journal of Computational and Nonlinear Dynamics*, vol. 3, no. 2, Article ID 021104, 10 pages, 2008.
[49] A. C. J. Luo, *Global Transversality, Resonance and Chaotic Dynamics*, World Scientific, Hackensack, NJ, USA, 2008.
[50] A. C. J. Luo, "A theory for flow switchability in discontinuous dynamical systems," *Nonlinear Analysis: Hybrid Systems*, vol. 2, no. 4, pp. 1030–1061, 2008.